Cell Death & Disease

https://doi.org/10.1038/s41419-026-08533-3

Article in Press

Dual inhibition of mTOR and HSP90 enhances cisplatin efficacy and overcomes resistance in ovarian cancer

Received: 1 August 2025

Revised: 9 February 2026

Accepted: 23 February 2026

Cite this article as: Lombardi, R., Addi, L., Pucci, B. *et al.* Dual inhibition of mTOR and HSP90 enhances cisplatin efficacy and overcomes resistance in ovarian cancer. *Cell Death Dis* (2026). https://doi.org/10.1038/s41419-026-08533-3

Rita Lombardi, Laura Addi, Biagio Pucci, Francesca Bruzzese, Maura Sonego, Anna Nespolo, Maria Serena Roca, Federica Iannelli, Luigi Alfano, Francesca Capone, Elena Di Gennaro, Gustavo Baldassarre & Alfredo Budillon

Combined inhibition of mTOR and HSP90 potentiates cisplatin antitumor effect and overcomes resistance in ovarian cancer

Rita Lombardi[2*], Laura Addi[1*], Biagio Pucci[1*], Francesca Bruzzese[2], Maura Sonego[3], Anna Nespolo[3] Maria Serena Roca[1], Federica Iannelli[1], Luigi Alfano[4], Francesca Capone[1#], Elena Di Gennaro[1], Gustavo Baldassarre[3], Alfredo Budillon[5§].

1. Experimental Pharmacology Unit, Istituto Nazionale Tumori Fondazione G. Pascale - IRCCS, Naples, Italy;
2. Experimental Animal Unit, Istituto Nazionale Tumori Fondazione G. Pascale - IRCCS, Naples, Italy;
3. Molecular Oncology Unit, Centro di Riferimento Oncologico di Aviano (CRO) IRCCS, National Cancer Institute, Aviano (PN), Italy;
4. Breast Unit, Istituto Nazionale Tumori Fondazione G. Pascale - IRCCS, Naples, Italy;
5. Scientific Directorate, Istituto Nazionale Tumori Fondazione G. Pascale - IRCCS, Naples, Italy.

[#]present addess: Laboratorio di Patologia Clinica, Azienda Ospedaliera di Rilievo Nazionale e di Alta Specialità San Giuseppe Moscati, Avellino, Italy;

*Rita Lombardi, Laura Addi and Biagio Pucci contributed equally to this article

§Corresponding Author: Alfredo Budillon, Istituto Nazionale per lo Studio e la Cura dei Tumori "Fondazione G. Pascale" – IRCCS, Via M. Semmola, 80131 Napoli, Italy. Phone: +39 081 5903292; E-mail: a.budillon@istitutotumori.na.it.

Keywords: Platinum resistance, HSP90, mTOR, phosphoproteomics, ovarian cancer

Funding. This work was supported by Italian Ministry of Health Ricerca Corrente and 5X1000 funds to Istituto Nazionale Tumori G. Pascale (RC projects 4/39_25 and 4/20_25; 5X1000_2021_1) and by the Associazione Italiana per la Ricerca sul Cancro (AIRC), Investigator Grant IG 26253 awarded to GB.

Abstract

Epithelial ovarian cancer (EOC) represents the most lethal gynecological disease, with a 5-year relative survival rate of 46% after the diagnosis. Standard treatment includes surgery followed by platinum (Pt)-based chemotherapy. However, Pt-resistance frequently occurs and strongly impact on the survival of EOC patients for whom we still do not have valid therapeutic options. By using a proteomic approach, we previously demonstrated a potential role of HSP90 in the mechanism of resistance in vitro, ex vivo e partially in vivo. To further investigate in depth the mechanism by which EOC cells acquired Pt-resistance, we used a quantitative phosphoproteomics approach followed by enrichment functional analysis. Here, we identified 542 differentially expressed phosphoproteins in Pt-resistant compared to parental cells identifying mTOR and HSF1 as the most enriched pathways. The up-regulation of the phosphorylated form of PDK1, AKT, mTOR and RPS6 was observed in Pt-resistant compared to parental cells. Moreover, we also demonstrated the up-regulation of the activity of HSF1 along with the elevation crucial components of the chaperone complex machinery HSP90, HSP70 and HSP40. Since mTOR is an attractive target for therapeutic intervention because of its key role in the crosstalk of various signalling pathways, we propose a novel therapeutic strategy based on the pharmacologic inhibition of HSP90 and mTOR able to further potentiate the Pt-based chemotherapy. Accordingly, the combination of ganetespib (an HSP90 inhibitor) and temsirolimus (a FDA approved-mTOR inhibitor) with cisplatin synergistically reduced colony formation and microtissues cell growth in vitro by increasing DNA-damage and apoptosis and in vivo enhancing mouse survival. Mechanistically, the triple combination treatment, impaired the proteins involved in mTOR signalling and HSF1 transactivation. Notably, all these data were confirmed also in Pt-resistant Non Small Cell Lung Cancer models. Collectively, our findings identify a promising new antitumor strategy for the treatment of Pt-resistance in cancer patients.

Introduction

The majority of cancer patients are still treated with chemotherapy (CT), either alone or in combination with radiotherapy, targeted therapies or immunotherapy [1]. Platinum (Pt) based drugs, including cisplatin (CDDP), carboplatin and oxaliplatin, are widely used in anticancer therapies [2]. To date, it is estimated that approximately 50% of all patients with cancer are treated with CDDP with significant clinical successes either when it is used as monotherapy, or in combination treatments [3]. In details, among others, CDDP-based therapies are approved for the treatment of epithelial ovarian cancer (EOC), non-small cell lung cancer (NSCLC) and head and neck squamous cell carcinoma (HNSCC) patients [4 5]. Unfortunately, relapses of acquired drug-resistant disease are common in advanced stages and have hampered CDDP clinical utility. Therefore, improving the clinical efficacy of CDDP and other Pt-based drugs has emerged as a critical unmet need for anticancer approaches and as a central goal for researchers worldwide in the fields of oncology and pharmacology.

EOC, which can be divided into high grade-serous ovarian cancer, endometrioid carcinomas, clear-cell carcinomas, mucinous carcinomas, and low-grade serous carcinomas represents the third most common and the most lethal gynaecologic malignant neoplasm worldwide with a 5-year relative survival rate of 46% after the diagnosis [6]. EOC are clinically classified as Pt-sensitive (~80% of the cases) and Pt-resistant disease based on the timing of response to first-line Pt-based therapy. For Pt-sensitive patients the addition of targeted therapies as concomitant or maintenance treatments has become a standard component of first-line therapies and significantly improved patients' survival [7 8]. However, more than half of all originally Pt-sensitive EOC patients experience Pt-resistant recurrences, that predicts poor overall survival and for which no effective treatments are available [9]. Indeed, also immunotherapies, that is efficacious in treatment of many other solid malignant neoplasms, have shown less promise for Pt-resistant EOC patients to date [10].

Pt-based chemotherapy is widely used as standard of care in different treatment setting for NSCLC patients lacking drug-targetable driver mutations (approximately 85–90%) [11]. Similarly, CDDP is probably the most widely used agent to treat squamous cell carcinoma of the head and neck (HNSCC) [12].

As observed in EOC also for NSCLC and HNSCC patients, the development of Pt-resistance predict slow survival rates and represents a pressing unmet clinical need.

Consequently, many studies focus on targeted approaches to understand the molecular mechanisms associated with the onset of Pt-resistance, with more attempts to the ovarian cancer treatment landscape [13].

The principal cytotoxic mechanism of CDDP involves the binding of Pt to DNA after its entry into tumor cells. Within the tumor cell, several mechanisms contribute to Pt- resistance, including reduced drug uptake, enhanced drug efflux, increased DNA damage repair and inactivated cell death signaling [14]. Our group has been studying for many years the molecular mechanisms underlying Pt-response and resistance and recently, using a proteomic approach, we have characterized the proteome of three CDDP-resistant isogenic high-grade EOC cell lines (TOV-112D Pt-res, MDAH-2774 Pt-res, and OVSAHO Pt-res) in comparison to their parental Pt-sensitive counterparts [15]. In detail, we identified the heat-shock protein 90 (HSP90) as a key player in the network of proteins differentially expressed between resistant and parental cells and demonstrated that the HSP90 inhibitor ganetespib exhibited a potent antitumor synergistic effect with CDDP in Pt-res EOC cells both *in vitro*, *ex vivo* and partially *in vivo* [15]. Notably, we obtained similar results in a Pt-res NSCLC isogenic model [16], suggesting that the same molecular mechanisms can operate in different tumour types treated with Pt-based therapies.

Here, to further investigate in depth the mechanisms underlying the acquired Pt-resistance in EOC, we took advantage of a phosphoproteomics approach highlighting Heat shock factor (HSF1) and mammalian target of rapamycin (mTOR) as main activated pathways in our EOC Pt-resistant cellular model. Our data

suggest the efficacy of a novel therapeutic strategy based on the combined pharmacologic inhibition of HSP90 and mTOR to further potentiate Pt-based chemotherapy and to revert Pt-resistance in EOC, NSCLC and HNSCC cells, substantiating the potential existence of a common mechanism across various tumor types.

Results

Phosphoproteomic analysis identified several differentially expressed proteins between Pt-resistant and parental EOC cells

Phosphorylation is one of the most relevant protein post-translational modifications and plays critical roles in the regulation of many cellular processes, including cell cycle, growth, apoptosis and signal transduction pathways [17].

Based on the notion that Pt-resistant cells differ from the Pt-sensitive counterpart in their total proteome, we decided to investigate more in depth these differences exploiting a LC-MS/MS phosphoproteomics approach to compare the expression profile of TOV-112D platinum resistant cells (TOV-112D Pt-res cl.7) to the sensible counterpart (TOV-112D) [18, 19, 20].

Principal component analysis (PCA) showed a good experimental reproducibility of phosphoproteomics results as demonstrated by the close relationship between the biological replicates, for each cellular model, into two groups corresponding to TOV-112D Pt-res cl.7 cells (red) *versus* (*vs*) parental cells (black) **(Figure 1A)**. Accordingly, the technical variability of each peptide/protein estimated using the Pearson correlation coefficients (Perseus software (v. 1.6.6.0), demonstrated high peptides/proteins reproducibility among biological replicates in parental (TOV-112D #1 *vs* TOV-112D #2) and resistant cells (TOV-112D Pt-res cl.7 #1 *vs*TOV-112D Pt-res cl.7 #2) while, TOV-112D #1 *vs* TOV-112D Pt-res cl.7 #1 had a lower correlation coefficient. **(Supplementary Figure 1A)**.

The analyses of 542 phosphoproteins using the Progenesis software (see methods for details) allowed the identification of proteins differentially expressed between sensitive and resistant cells (**data availability statement doi: 10.5281/zenodo.16564396)** and their classification according to the gene ontology (GO) database and pathway analysis. Both g-Profiler and DAVID software used for data analyses highlighted mTOR as one of the main differentially expressed pathways **(Figure 1B-D and Supplementary Figure 1B)**.

In accord with a possible pivotal involvement of mTOR pathway in differentiate Pt-sensitive and resistant cells we also observed HSF1 dependent transactivation and protein folding chaperone and PI3K-Akt signaling pathways as differentially enriched in the two models **(Figure 1B-C)** [21].

Finally, functional annotation clustering showing the number of proteins related to the ontology categories (DAVID software) and volcano plot analyses confirmed the increase of mTOR, HSF1 and HSP90 activity in TOV-112D resistant cells **(Figure 1D and Supplementary Figure 1C)**.

The PI3K/mTOR pathway **(Figure 2A)** is a central hub involved in the regulation of proliferation, progression, metastasis and chemo-resistance of tumor cells [22], and several lines of evidence suggest that the mTOR pathway is intricately linked to the activity of the transcription factor HSF1. Specifically, mTOR could directly phosphorylate HSF1, promoting its activation, nuclear translocation and heat shock proteins transcription [21].

Therefore, based our phospho-proteomic data and the current literature we decided to better investigate the role of PI3K/mTOR/HSF1 axis in Pt-sensitive and resistant TOV-112D cells trying to understand if this axis could represent a specific vulnerability of Pt-resistant tumors.

First, we validated phospho-proteomic data using western blot analyses confirming that TOV-112D Pt-res cl. 7, compared to parental cells, had increased expression of the phosphorylated forms of PDK1, AKT, mTOR, p70S6K and RPS6, all protein members of the PI3K/mTOR signaling pathway **(Figure**

2B). Moreover, TOV-112D Pt-res cells showed an increased expression of the activating phosphorylation of HSF1 and of its targets heat shock proteins HSP90, HSP70 and HSP40, which are crucial components of the protein folding chaperone complex **(Figure 2C and 2D)**. Interestingly, among the differentially expressed proteins, we identified by phosphoproteomics approach and validated by western blot the kinase DYRK2 known as client of HSP90 and able to phosphorylate HSF1 **(Figure 2C)** [23].
Importantly, the expression of HSP90, phosphorylated HSF1 and with a lesser extent phosphorylated mTOR were confirmed in primary culture obtained from Pt-sensitive and Pt-resistant EOC patients, confirming the clinical relevance of the preclinical results **(Figure 2E)**.
These data are in complete accord with our previous observation indicating that HSP90 is a critical hub within a network of differentially expressed proteins identified in a Pt-res non-small cell lung cancer (NSCLC) isogenic model (A549 CPr) [16].
Indeed, NSCLC Pt-resistant model cells A549 CPr showed an hyper-activation of the protein involved in mTOR mediated signaling pathway, HSF1 dependent transactivation and chaperone complex when compared with the Pt-sensitive A549 counterpart **(Supplementary Figure 2A-C)**, hypothesizing that similar mechanisms are present in different tumor types.
Based on our previous results demonstrating that HSP90 inhibition synergistically improve the antitumor activity of CDDP *in vitro* and *ex vivo* in primary cultures derived from the ascites of Pt-res EOC patients [15], we exploited the CRISPR-Cas9 system to generated knockout HSP90α cells (A549 CPr KO#1, #3, #4) from A549 CPr **(Supplementary Figure 3A)**. Using these tools we confirmed in a NSCL model that HSP90α knockout partially reversed Pt-resistance, as verified by colorimetric cytotoxicity assay **(Supplementary Figure 3B)**, colony formation assay **(Supplementary Figure 3C)**, and induction of apoptosis evaluated by PARP cleavage **(Supplementary Figure 3D)**.
Complementary to the knockout studies, we performed HSP90α knock-in experiments **(Supplementary materials and methods)** in the platinum-sensitive TOV-112D cell lines **(Figure 3A)**. Clonogenic assays revealed that HSP90α-overexpressing cells exhibited reduced sensitivity to CDDP compared to empty vector controls **(Figure 3B)**. Moreover, these cells did not display induction of apoptosis or DNA damage upon CDDP treatment, as evaluated by Annexin V staining **(Figure 3C)** and γH2AX Western blot analyses **(Figure 3D)**. These results further support the pivotal role of HSP90 in modulating platinum resistance.Overall, the collected data support the possibility that acquired Pt-resistance induce a tumor agnostic upregulation of the PI3K/mTOR/HSF1 axis that leads to the overexpression of HSPs chaperone proteins and that this axis might represent a specific vulnerability of Pt-res cells.

HSP90 and mTOR inhibitors potentiate CDDP antitumor effect and reverse Pt-resistance

Our present and previous data support the notion that inhibition of HSP90 protein ameliorate the activity of platinum in EOC *in vitro* also in the context of Pt-resistant disease but also demonstrated that the Pt plus ganetespib is only partially active *in vivo* in Pt-res EOC xenograft models [15]. This evidence is in line with the results of clinical trial using ganetespib as a single agent or in combination with chemotherapy in different type of human cancers, showing no improvement of patient survival [24 25 26]. In the context of Pt-resistant EOC patients the use of ganetespib in combination with chemotherapy is feasible, although with limited clinical utility even if we have to wait for the results of the activity GANNET53 Phase I/II trial, which will give a final answer on its clinical activity [27 28].
These preclinical and clinical data suggest that, although HSP90 inhibitors are manageable drugs with potential clinical activity, novel therapeutic strategies should be tested to improve its efficacy toward its clinical translation in the context of chemo-resistant tumors.
Our data showing high levels of mTOR in Pt-res relative to parental cells and the wide use of mTOR inhibitors in several type of cancer with discrete success and manageable toxicities, suggested us that it might also represent a potential therapeutic target in Pt-res EOC setting.

Based on these considerations, we explored the efficacy of a novel therapeutic strategy through the pharmacologic inhibition of HSP90 and mTOR both putatively able to improve the Pt-based chemotherapy.

To this aim, we evaluated the combination of the inhibitors of HSP90 (ganetespib) and mTOR (temsirolimus) plus CDDP in Pt-sensitive and resistant EOC and NSCLC models. We first tested the sensitivity of cell lines to single agent treatment, demonstrating a cross-resistance of Pt-resistant cells to ganetespib and temsirolimus **(Supplementary Table 1)**.

We then investigated the combination of CDDP with ganetespib and/or temsirolimus using equipotent doses and evaluated the CI values calculated at 50% (CI50), 75% (CI75) and 90% (CI90) of cell lethality, in TOV-112D parental and resistant cells. By considering strong synergism CI $\leq$ 0.8, synergism CI $\leq$ 0.9, additivity CI > 0.9 and $\leq$ 1.1, and antagonism CI > 1.1 [29], we obtained consistent synergistic antiproliferative effects and strongest effects using the triple combination **(Figure 4A and Supplementary Table 2)**.

The synergistic interaction between the three drugs was then confirmed by evaluating the doses reduction index (DRIs) for CDDP, which represent the order of magnitude (fold) of dose reduction obtained for the IC50 (DRI_{50}) of each agent in combination *vs* single drug treatments **(Figure 4B)**. Importantly, we extended our analysis to an additional EOC model, OVCAR8 and its platinum-resistant counterpart (OVCAR8 Pt.res cl.2), which represents the high-grade serous ovarian cancer subtype, the most prevalent histological form of the disease. We obtained consistent synergistic antiproliferative effects and strongest effects using the triple combination (**Supplementary Figure 4 and Supplementary Table 2**). These results further confirmed that concurrent inhibition of HSP90 and mTOR enhances the efficacy of platinum-based chemotherapy. Moreover, we demonstrated that concomitant treatment with CDDP/ganetespib/temsirolimus completely suppressed colony formation in TOV-112D parental and Pt-resistant cells using the IC_{10}^{96h} dosages of parental cells **(Figure 4C, Supplementary Figure 5A and Supplementary materials and methods)**.

Although two-dimensional (2D) monolayer *in vitro* models are time and cost efficient, they lack the complexity of intact physiological systems and may not provide results that can be correlated with *in vivo* responses [30].

Three-dimensional (3D) *in vitro* platforms provide a unique alternative to bridge the gap between traditional 2D *in vitro* and *in vivo* models [31].

On this regard, we showed by 3D microtissue assay, using NIH/3T3 fibroblast cell line isolated from mice as scaffold and ovarian cancer cells as tumor component, that CDDP/ganetespib/temsirolimus combination led to a potent microtissues regression especially in TOV-112D Pt-res cl. 7 cells, compared to single and double treatments using IC_{50}^{96h} dosages of parental cells **(Figure 4D)**.

We observed that the potentiation of CDDP antitumor effect by ganetespib plus temsirolimus was likely due to an increased apoptosis as demonstrated by the evaluation of Annexin V positivity cells **(Figure 5A, Supplementary Figure 5B and Supplementary materials and methods)** and of cleaved PARP1 **(Figure 5B and Supplementary Figure 5C)** expression. The increase apoptosis was accompanied by a clear induction of DNA damage when the CDDP/ganetespib/temsirolimus was used (i.e. γH2AX expression) compared to single and double treatments using IC_{50}^{96h} dosages of parental cells **(Figure 5C and Supplementary Figure 5D)**.

Notably, similar synergism by the combination of ganetespib and temsirolimus plus CDDP was observed in A549 CPr model, particularly when the triple combination was tested **(Supplementary Figure 6A and Supplementary Table 3)**. The DRI_{50} evaluation for CDDP and the colony formation assays using IC_{10}^{96h} dosages of parental cells confirmed these **(Supplementary Figure 6B-C)**. Also in the NSCLC model, the anticancer activity of the triple combination was associate to an increase in apoptosis as showed by the evaluation of Annexin V positivity **(Supplementary Figure 6D)**.

Finally, we demonstrated the synergistic anti-proliferative effect of the triple combination in Head and Neck intrinsic Pt-resistant Cal27 and Cal33 cell lines, evaluating first the sensitivity of cell lines to single agent treatment **(Supplementary Table 4-5 and Supplementary Figure 7A-B)**. Notably, 3D visualization of the Cal27-GFP+/Luc+ cells highlighted the impact of all treatments on cell mean volume, particularly of the triple combination **(Supplementary Figure 7C)**.

Mechanistically, we showed by western blot that the triple combination decreased the expression and the activation of the main proteins involved in mTOR signaling pathway, HSF1 transactivation and chaperone complex in TOV-112D Pt-res cl. 7 cells **(Figure 6A-C)**. These data were also confirmed in A549 CPr model, supporting the possibility that the same mechanism is present in different tumor types **(Supplementary Figure 8A-C)**. Notably, phosphoprotein analysis at 24 hours in TOV-112D Pt-res cl.7 and A549 CPr cells revealed an early down-modulation, indicating that the triple combination rapidly interferes with key signaling cascades and exerts its effects already at early time points **(Supplementary Figure 9 A-B)**, which become further pronounced at 48 hours (**Figure 5 A-B and Supplementary Figure 8A-B)**.

***In vivo* synergistic antitumor effect of ganetespib, temsirolimus and CDDP combination**

To evaluate the relevance of in *vitro* results we used the CDDP/ganetespib/temsirolimus combination to treat NSG mice-bearing tumours formed by TOV-112D Pt-res cl.7 cells (**Figure 7A**). When tumors reached ~ 100 mm^3 of volume, mice were randomized in four treatment groups: control, temsirolimus, CDDP plus ganetespib and CDDP plus ganetespib and temsirolimus. Significantly, as shown in Figure 6, the triple combination treatment almost completely block tumour growth compared with the other experimental groups **(Figure 7B)**. We observed a modest decrease of mice body weight in the triple combination treatment; however, it was less than 10% and was not paralleled by other signs of acute or delayed toxicity **(Figure 7C)**. The synergistic effect of the CDDP/ganetespib/temsirolimus combination treatment was confirmed by the resulting tumour growth delay (TGD) that reached a peak of about 45% indicating that the mean rate of tumour growth was more than four-fold higher in the controls or the treated groups, than the combination setting **(Figure 7D)**. Moreover, by calculating the percent change in tumour volume from the time of initial treatment (day 3) to day 28, we demonstrated that temsirolimus, CDDP plus ganetespib and the triple combination treatment reduced the tumour burden by about 15, 30, and 85%, respectively **(Figure 7E)**. The reduced tumor growth also translated in a significant improvement of mice survival in the triple combination group, as demonstrated by Kaplan-Meier plot reported in **Figure 7F**.

Finally, we confirmed the synergistic interaction of the proposed combination in A549 CPr cells xenograft model in athymic mice confirming that the triple combination lead to a reduction of the tumour volume compared with controls or other treated groups and a TGD that reached a peak of more than 100% (**Supplementary Figure 10A-C)**.

Overall our data demonstrated the efficacy and feasibility of CDDP plus ganetespib and temsirolimus combination in potentiating the antitumor effect of CDDP and to revert Pt-resistance *in vivo* in different tumour models.

Discussion

Platinum (Pt)-based compounds are among the most commonly used chemotherapeutic agents to treat a wide variety of tumors and since their introduction into clinical practice, numerous omics-based studies have been conducted to address the clinically significant challenge of Pt resistance that critically limits their efficacy [32, 33].

However, many of these studies have suffered from a major limitation due to the imprecise correlation between gene and protein expression, resulting in difficulty in identifying new effective therapeutic targets to overcome resistance [34]. Conversely, comprehensive analyses of the global proteome and phosphoproteome could provide new insights into the molecular mechanisms of chemoresistance and contribute to the identification of new biomarkers or therapeutic targets [35, 36]. Indeed, in the present study, by using a quantitative phosphoproteomics-based approach coupled with database analysis and bioinformatics tools, we identified the mammalian target of rapamycin (mTOR) and Heat Shock Factor 1 (HSF1)-activated multichaperone complex (HSP90, HSP70, and HSP40) as possible activated pathways by which cells acquire platinum chemoresistance. Notably, we validated the activation and the up-regulation of the main identified proteins involved in the pathways in both EOC and NSCLC Pt-res resistant models.

The present study followed our experiences demonstrating, in line with others, that the multifunctional molecular chaperone HSP90, represents a central therapeutic hub in Pt-resistant EOC and NSCLC [15, 16]. Although we have clearly demonstrated the ability of the HSP90 clinically active inhibitor ganetesbip to synergize with CDDP in Pt-resistant EOC *in vitro* and *ex vivo* preclinical models, the antitumor effect of the combination in *in vivo* models, was less effective than expected [15]. HSP90 by regulating the post-translational stability and function of a distinct but diverse set of "client" proteins, known to be critically involved in oncogenesis is an appealing target for cancer therapy. High expression of HSP90 is associated with tumor growth and , inhibiting HSP90 activity has proven to disrupt multiple signal transduction pathways that are important for tumor development and survival [37]. Despite the extensive evaluation of HSP90 inhibitors (HSP90i) in clinical trials, none have received FDA approval, largely due to drug-related toxicity or therapy resistance as single agents. Notably, the two recently completed no-proft clinical studies investigating in ovarian cancer patients the combination of ganetespib in combination with either paclitaxel in PT-resistance setting [38] [27] or with carboplatin followed by maintenance treatment with the PARP inhibitor Niraparib, in PT-sensitive setting [39], have both shown no improved outcome, suggesting novel strategies to enhance the antitumor therapeutic response of this class of agents [40]. In this context, our work demonstrating the synergy between HSP90 and mTOR inhibition, might indicate a novel clinical possibility based on a solid molecular rationale.

The dysregulation of mTOR has been implicated in tumorigenesis, metastasis and drug resistance across various human cancers [22, 41]. HSF1 is a master regulator responsible for inducing the expression of heat shock proteins (HSPs) and PI3K-AKT-mTOR oncogenic pathway activation [21].

Given the pivotal role of mTOR in coordinating various signaling pathways, it has been proposed as an attractive therapeutic target in cancer treatment [42]. The mTOR inhibitors function as antiproliferative drugs; however, as single agents, they have demonstrated limited efficacy in tumor eradication due to the activation of compensatory survival pathways. Nonetheless, mTOR inhibition has been shown to enhance the efficacy of various chemotherapeutic agents, including CDDP, carboplatin, paclitaxel, and doxorubicin, across different tumor types [43, 44]. In line with this, temsirolimus, a potent and selective inhibitor of mTOR, was approved by the European Medicines Agency for the treatment of relapsed/refractory Non-Hodgkin's Lymphoma (Mantle Cell Lymphoma)[45] and by US Food and Drug Administration for poor prognosis metastatic renal cell carcinoma (mRCC) [46].

A phase II trial evaluating temsirolimus in combination with carboplatin and paclitaxel followed by temsirolimus consolidation in women with newly diagnosed clear cell ovarian cancer (CCOC), although

well tolerated did not statistically significantly increase PFS at 12 months compared to historical controls [47]. Similarly, in women with Pt-refractory/resistant ovarian cancer or advanced/recurrent endometrial carcinoma, temsirolimus did not meet the predefined efficacy criteria and few patients had long lasting disease stabilizations [48]. Conversely, based on our phosphoproteomics findings, here we demonstrated that triple combination of ganetespib and temsirolimus plus CDDP significantly enhanced the response to CDDP both *in vitro* and *in vivo* in Pt-resistant EOC and NSCLC xenograft models compared to single or double treatments. These data were also confirmed *in vitro* in HNSCC models. To our knowledge this is the first study evaluating the combination of an HSP90i such as ganetespib and temsirolimus in cancer models and the first to show the reversion of Pt-resistance by this original combination. Interestingly, mechanistically, this effect is linked to increased pro-apoptotic signaling and DNA damage, suggesting that targeting both mTOR and HSP90 disrupts critical survival pathways in Pt-resistant cells. In this regard, it has been demonstrated that mTOR inhibition activates autophagy to mediate the degradation of anti-apoptotic B cell lymphoma 2 (Bcl-2) protein to induce apoptosis [49]. Moreover, mTOR plays also a crucial role in the cellular response to CDDP by regulating apoptosis. In detail, a combination of the mTOR inhibitor rapamycin and the PI3K inhibitor LY294002 with CDDP has been shown to increase apoptosis and inhibit tumor growth in melanoma, correlating with the downregulation the anti-apoptotic protein Mcl-1 [50]. We also demonstrated that the triple combination treatment impaired proteins involved in mTOR signaling and the HSF1-activated multichaperone complex pathway, suggesting their potential association with off-target Pt-resistance mechanisms, along with other well-known pathways including autophagy, epigenetic changes, cancer stem cells (CSCs), epithelial-mesenchymal transition (EMT), and the heat shock response (HSR) [51]. Overall, our data support the possibility that the multimodal mechanisms of Pt-resistance acquisition in different cancer cellular models, which differ in histology and genetic backgrounds, are commonly dependent on the addiction, at least in part, to HSP90 and mTOR hub function.

In line with our data, in recent years, it has been proven that combining Hsp90 and mTOR inhibitors or dual HSP90-mTOR inhibitors could produce synergistic anti-cancer activity in various tumor such as cholangiocarcinoma, breast carcinoma, melanoma and bladder cancer [52].

Although further studies should focus on better elucidating the molecular mechanisms underlying the synergistic antitumor effect of Hsp90 and mTOR inhibitors plus CDDP, our data provided a rationale to clinically explore this combination in CDDP refractory/resistant cancer patients. This combination treatment could have higher antitumor effects tested in patient stratified/selected, based on the evaluation of biomarkers within mTOR signaling and HSF1-HSP90 regulatory pathway, as suggested by our molecular findings.

Materials and Methods

Cell culture conditions and cisplatin-resistant cell selection

TOV-112D (CRL-11731), NSCLC cell line A549 (CCL-185) and Cal33 (CVCL-1108) were purchased from ATCC (Manassas, VA, USA). CAL27 (CRL-2095) cell line was kindly provided by Dr. J. L. Fishel (Centre Lacassagne, Nice, France).

OVCAR-8 cells were purchased from National Cancer Institute Developmental Therapeutics Program Tumor Repository (Frederick, Maryland, USA). The green fluorescent protein+/luciferase+ (GFP+/Luc+) Cal27 cell line were obtained by lentiviral infection as described previously [53].

TOV-112D CDDP-resistant cancer cells (referred as TOV-112D Pt-res cl-7), OVCAR 8 CDDP-resistant cancer cells (referred as OVCAR 8 Pt-res cl-2) and A549 CDDP-resistant cancer cells (CPr-A549) were generated as previously described [18, 19, 20 16]. More details are described in Supplementary materials and methods.A549 heat-shock protein 90 alpha isoform (HSP90α) knockout cells were generated through the CRISPR-Cas9 system as reported previously [54] . The generated cell clones (A549CPr KO#1, KO#3, KO#4) were analyzed by western blot and sequencing to verify knockout of HSP90α.

Patient-derived primary cells were described in [55] [56] and were obtained from patients who gave their informed consent, under protocols approved on 10.07.2019 by the Ethics Committee (OutCoME protocol - CRO-2019-53 approval CEUR 2019-Sper-084). The experiments were conformed to the principles set out in the WMA Declaration of Helsinki and the Department of Health Services Belmont Report. Patient data were pseudonymized and annotated in a prospective database. Primary cells were maintained in OCMI medium (M199 and Ham's 1:1) supplemented with 2% FBS, EGF (10 ngmL−1), hydrocortisone (500 ngmL−1), cholera toxin (25 ngmL−1), and insulin (20 μMmL−1).
All cell lines were regularly inspected for mycoplasma. The cells have been authenticated with short tandem repeat profile generated by LGC Standards.

Label free MS-based phosphoproteomics quantitation

In-solution digestion and phosphopeptide enrichment was performed. Purification of phosphopeptides was performed. Briefly, tryptic peptides were diluted six-fold in 80% (v/v) ACN, 6% (v/v) TFA (loading solution) and applied to TiO_2 beads (about 50 μl slurry) pre-equilibrated in loading buffer and incubated for 15 min a room temperature in a Thermo-mixer R at a speed of 300 rpm. The samples were then washed three times with 50 μl of 80% ACN, 0.1% TFA (wash solution). Finally phosphopeptides were eluted with 100 μl of elution solution 1 (20 μl of 25% ammonium hydroxide solution [pH≥ 10.5] + 980 μl H_2O) followed by 100 μl of elution solution 2 (30% ACN). Both eluted 1 and 2 were dried in vacuum system (Concentrator 5301, Eppendorf, Milan, Italy). Samples were desalting by stage Tip C18 (Millipore, Merck KGaA, Munich, Germany) and lyophilized again. Desalted fractions were resuspended in 20 μl (approximately 5 μg of peptides) of 0.1% TFA and injected into Dionex UltiMate 3000 Rapid Separation LC nano system (Thermo Fischer Scientific, CA, USA) coupled with an AmaZon ETD mass spectrometer (Bruker Daltonics, Bremen, Germany). More details are described in Supplementary materials and methods.

Phosphoproteomics quantification analysis

Progenesis QI for proteomics v. 4.2 (Non-linear Dynamics, Newcastle, England) was used as label-free quantification platform as previously described [57] [58]. The details are described in Supplementary materials and methods.Technical variability of each peptide/protein was estimated among replicates from the pooled sample by calculating Pearson correlation coefficients using the Perseus (v. 1.6.6.0) [59].

Bioinformatic analysis

KEGG pathway, Functional Annotation Clustering and Gene Ontology Biological Process (GO-BP) analyses were performed using the Database for Annotation, Visualization and Integrated Discovery (DAVID) v6.8 (https://david.ncifcrf.gov/) using as background the *Homo Sapiens* proteome [60]. Enrichment of GO terms was considered statistically significant when corrected for multiple testing by the Benjamini-Hochberg method with adjusted $p < 0.05$. Pearson correlation analysis and volcano plot were calculated using the Perseus (v. 1.6.6.0) as reported by Tyanova et al. [59]. G:Profiler (version e94_eg41_p11) was performed as follows: Homo Sapiens was chosen as organism, GO analyses (GO molecular function (GO: MF) and GO cellular component (GO: CC), were carried out sequentially. The biological pathways were evaluated by Reactome (REAC) and WikiPathways (WP) databases. The statistical domain scope was used only for annotated genes. The significance threshold was the g:SCS threshold. The user threshold was $p<0.05$ [61].

Immunoblotting

Protein extraction after 48h of cell culture and immunoblotting was performed as previously described [15]. Western blots were quantified using IMAGEJ software (Rasband, W.S., U.S., National Institutes of Health, Bethesda, MD, USA). For primary and secondary antibodies see Supplementary materials and methods.

Cell proliferation assay and drug combination studies

cis-Diammine Pt (II) dichloride (CDDP) was provided by Sigma-Aldrich (St. Louis, MO, USA); Ganetespib was provided by MedChem Express (Sollentuna, Sweden) and stock solutions were prepared in DMSO. Temsirolimus (Torisel®) was provided by Pfizer. Cell viability and combination studies were measured using SRB assays after 96h of treatment in 96-well plates, as described previously [15, 62].

Microtissue formation assay

Ovarian cancer cell lines TOV-112D and TOV112D Pt-res cl.7 (800 cells) and Head and Neck Cal27-GFP^+/Luc^+ cancer cells (500 cells) were cultured as microtissues by the ultra-low attachment (ULA) System (PerkinElmer, Waltham, Massachusetts, USA). The ovarian cancer cells were marked using a green fluorescent probe-cell traker (Thermo Fisher Scientific, Waltham, Massachusetts, USA). The 3D microtissue model for the EOC cell lines was obtained using mouse fibroblast cells NIH/3T3 as scaffold in a ratio of 3:1 as described in literature and untreated or treated with drugs, for 96h with CDDP, ganetespib and temsirolimus alone or in combination at IC_{50}^{96h} doses of parental cells. 3D microtissues were maintained in the incubator and photographed by Opera Phenix microscope (PerkinHelmer, Waltham, Massachusetts, USA) air objective magnification 5X and scored by Cell Titer-Glo® 3D Cell Viability Assay (Promega, Madison, Wisconsin, USA) by using a Multimode Reader Cytation 5 (Biotek, Santa Clara, California, USA).

In vivo xenograft studies

All studies have been performed in compliance with institutional guidelines and regulations that cover all scientific procedures involving the use of live animals (Directive 2010/ 63/EU; Italian Legislative Decree DLGS 26/2014).

Female NOD scid gamma (NSG) mice (4–6 weeks old) and female athymic (nude) mice (4–6 weeks old) were acquired from Charles River Laboratories (Charles River, Wilmington, MA, USA) and used for TOV-112D Pt-res cl.7 and A549 CPr xenograft model, respectively. Mice were acclimatized in the Animal Care Facility of 'Fondazione G. Pascale'-IRCCS/Laboratori di Mercogliano-CROM and housed in a 12 h light: 12 h dark cycle in a controlled room temperature of 22 ± 2 °C and fed ad libitum. After 3 days, TOV-112D Pt-res cl.7 cells (6×10^6) diluted in 200 mL [PBS/Matrigel GF (Becton Dickinson, Franklin Lakes, NJ, USA) 1/1] were injected subcutaneously (s.c) in flank regions of the mice. When the tumors became palpable, the mice were randomized into four experimental groups (n = 7). Intraperitoneal (i.p.) treatments were performed with temsirolimus (20 mg·kg−1, dissolved in 10% DMSO + 40% poly (ethylene glycol) + 5% TWEEN80 + 45% physiological solution) or CDDP (2.5 mg·kg−1, dissolved in PBS) and ganetespib (GANE; 30 mg·kg−1, dissolved in 10% DMSO + 40% poly (ethylene glycol) + 5% TWEEN80 + 45% physiological solution) or triple CDDP/ganetespib/temsirolimus combination, or vehicles, once a week.

A549 CPr cells (5×10^6) were injected s.c in flank region of the nude mice. When the tumors became palpable, the mice were randomized into eight experimental groups (n= 7). I.p. treatments were performed

with CDDP (2.5 mg·kg−1) and/or ganetespib (75 mgkg−1) and/or temsirolimus (20 mg·kg−1) or vehicles, once a week. Mice in the control groups were treated with both PBS and 10% DMSO + 40% poly (ethylene glycol) + 5% TWEEN80 + 45% physiological solution.
Sample size was based on estimations by power analysis with a level of significance of 0.05 and a power of 0.8 (G*Power version 3.1.9.7).
We took adequate steps to insure that animals did not suffer unnecessarily at any stage of the experiment described above.
Tumor volume (mm^3), tumor growth delay (TGD) and the percent change in tumor volume from the time of initial treatment to the end of the study were evaluated as described before [63]. Overall survival were calculated considering as positive event in Kaplan-Meier curves the achievement of humane end point (Volumetric cut-off:1500cm^3; Weight cut-off: 20% reduction).

Statistical analysis

The statistics of the shotgun proteomics experiment is performed by Progenesis QI for proteomics v. 4.2 and reported in the specific section.
Graphs and data analyses were carried out utilizing PRISM software (version 9, GraphPad, Inc., Ritme Informatique, Paris, France). Where the means of two data sets were compared, and significance was determined by a two-tailed Students t-test or ANOVA, as indicated in each figure. Differences was considered significant at $p < 0.05$ (* $p \leq 0.05$, ** $p \leq 0.01$, *** $p \leq 0.001$, **** $p \leq 0.0001$).

Acknowledgements

This work was supported by Italian Ministry of Health Ricerca Corrente and 5X1000 funds to Istituto Nazionale Tumori G. Pascale (RC projects 4/39_25 and 4/20_25; 5X1000_2021_1) and by the Associazione Italiana per la Ricerca sul Cancro (AIRC), Investigator Grant IG 26253 awarded to GB.

Declarations: The authors declare no conflict of interest.

Authors Contributions:

Lombardi R, Addi L, Pucci B, Bruzzese F, Di Gennaro E, Baldassarre G, Budillon A **conception and design of the study**
Lombardi R, Addi L, Pucci B, Sonego M, Nespolo A, Roca MS, Iannelli F, Alfano L, Capone F **data acquisition**
Lombardi R, Addi L, Pucci B, Bruzzese F, Di Gennaro E, Baldassarre G, Budillon A **analysis and interpretation of data;**
Budillon A, Di Gennaro E, Bruzzese F **resources**
Bruzzese F, Di Gennaro E, Baldassarre G, Budillon A **supervision;**
Budillon A, Di Gennaro E, Bruzzese F **funding acquisition;**
Lombardi R, Addi L, Pucci B, Bruzzese F, Di Gennaro E, Baldassarre G, Budillon A **wrote the paper;**
Lombardi R, Addi L, Pucci B, **graphed the data.**

All the authors revised the paper, contributed to the material and methods section, and edited the figures. All authors have read and approved the final manuscript.

Data Availability:

The raw data generated in this study are publicly available in Zenodo (**doi: 10.5281/zenodo.16564396**). All datasets are available from the corresponding author on reasonable request

References

1. Letai A, de The H. Conventional chemotherapy: millions of cures, unresolved therapeutic index. *Nat Rev Cancer* 2025, **25**(3)**:** 209-218.

2. Zhang C, Xu C, Gao X, Yao Q. Platinum-based drugs for cancer therapy and anti-tumor strategies. *Theranostics* 2022, **12**(5)**:** 2115-2132.

3. Ghosh S. Cisplatin: The first metal based anticancer drug. *Bioorg Chem* 2019, **88:** 102925.

4. Hack J, Crabb SJ. Platinum-Based Chemotherapy 'Rechallenge' in Advanced Non-ovarian Solid Malignancies. *Clin Oncol (R Coll Radiol)* 2022, **34**(8)**:** e329-e344.

5. Zon A, Bednarek I. Cisplatin in Ovarian Cancer Treatment-Known Limitations in Therapy Force New Solutions. *Int J Mol Sci* 2023, **24**(8).

6. Richardson DL, Eskander RN, O'Malley DM. Advances in Ovarian Cancer Care and Unmet Treatment Needs for Patients With Platinum Resistance: A Narrative Review. *JAMA Oncol* 2023, **9**(6)**:** 851-859.

7. Gogineni V, Morand S, Staats H, Royfman R, Devanaboyina M, Einloth K*, et al.* Current Ovarian Cancer Maintenance Strategies and Promising New Developments. *J Cancer* 2021, **12**(1)**:** 38-53.

8. Bartoletti M, Pelizzari G, Gerratana L, Bortot L, Lombardi D, Nicoloso M*, et al.* Bevacizumab or PARP-Inhibitors Maintenance Therapy for Platinum-Sensitive Recurrent Ovarian Cancer: A Network Meta-Analysis. *Int J Mol Sci* 2020, **21**(11).

9. McMullen M, Madariaga A, Lheureux S. New approaches for targeting platinum-resistant ovarian cancer. *Semin Cancer Biol* 2021, **77:** 167-181.

10. Pujade-Lauraine E, Fujiwara K, Ledermann JA, Oza AM, Kristeleit R, Ray-Coquard IL*, et al.* Avelumab alone or in combination with chemotherapy versus chemotherapy alone in platinum-resistant or platinum-refractory ovarian cancer (JAVELIN Ovarian 200): an open-label, three-arm, randomised, phase 3 study. *Lancet Oncol* 2021, **22**(7)**:** 1034-1046.

11. Fennell DA, Summers Y, Cadranel J, Benepal T, Christoph DC, Lal R*, et al.* Cisplatin in the modern era: The backbone of first-line chemotherapy for non-small cell lung cancer. *Cancer Treat Rev* 2016, **44:** 42-50.

12. Chow LQM. Head and Neck Cancer. *N Engl J Med* 2020, **382**(1)**:** 60-72.

13. Berek JS, Renz M, Kehoe S, Kumar L, Friedlander M. Cancer of the ovary, fallopian tube, and peritoneum: 2021 update. *Int J Gynaecol Obstet* 2021, **155 Suppl 1**(Suppl 1)**:** 61-85.

14. Amable L. Cisplatin resistance and opportunities for precision medicine. *Pharmacol Res* 2016, **106:** 27-36.

15. Lombardi R, Sonego M, Pucci B, Addi L, Iannelli F, Capone F*, et al.* HSP90 identified by a proteomic approach as druggable target to reverse platinum resistance in ovarian cancer. *Mol Oncol* 2021, **15**(4)**:** 1005-1023.

16. Milone MR, Lombardi R, Roca MS, Bruzzese F, Addi L, Pucci B*, et al.* Novel pathways involved in cisplatin resistance identified by a proteomics approach in non-small-cell lung cancer cells. *J Cell Physiol* 2019, **234**(6)**:** 9077-9092.

17. Minic Z, Dahms TES, Babu M. Chromatographic separation strategies for precision mass spectrometry to study protein-protein interactions and protein phosphorylation. *J Chromatogr B Analyt Technol Biomed Life Sci* 2018, **1102-1103:** 96-108.

18. Sonego M, Pellizzari I, Dall'Acqua A, Pivetta E, Lorenzon I, Benevol S*, et al.* Common biological phenotypes characterize the acquisition of platinum-resistance in epithelial ovarian cancer cells. *Sci Rep* 2017, **7**(1)**:** 7104.

19. Sonego M, Poletto E, Pivetta E, Nicoloso MS, Pellicani R, Vinciguerra GLR*, et al.* TIMP-1 is Overexpressed and Secreted by Platinum Resistant Epithelial Ovarian Cancer Cells. *Cells* 2019, **9**(1).

20. Lorenzon I, Pellarin I, Pellizzari I, D'Andrea S, Belletti B, Sonego M*, et al.* Identification and Characterization of a New Platinum-Induced TP53 Mutation in MDAH Ovarian Cancer Cells. *Cells* 2019, **9**(1).

21. Home T, Jensen RA, Rao R. Heat shock factor 1 in protein homeostasis and oncogenic signal integration. *Cancer Res* 2015, **75**(6)**:** 907-912.

22. Panwar V, Singh A, Bhatt M, Tonk RK, Azizov S, Raza AS*, et al.* Multifaceted role of mTOR (mammalian target of rapamycin) signaling pathway in human health and disease. *Signal Transduct Target Ther* 2023, **8**(1)**:** 375.

23. Moreno R, Banerjee S, Jackson AW, Quinn J, Baillie G, Dixon JE*, et al.* The stress-responsive kinase DYRK2 activates heat shock factor 1 promoting resistance to proteotoxic stress. *Cell Death Differ* 2021, **28**(5)**:** 1563-1578.

24. Goyal L, Chaudhary SP, Kwak EL, Abrams TA, Carpenter AN, Wolpin BM*, et al.* A phase 2 clinical trial of the heat shock protein 90 (HSP 90) inhibitor ganetespib in patients with refractory advanced esophagogastric cancer. *Invest New Drugs* 2020, **38**(5)**:** 1533-1539.

25. Pillai RN, Fennell DA, Kovcin V, Ciuleanu TE, Ramlau R, Kowalski D*, et al.* Randomized Phase III Study of Ganetespib, a Heat Shock Protein 90 Inhibitor, With Docetaxel Versus Docetaxel in Advanced Non-Small-Cell Lung Cancer (GALAXY-2). *J Clin Oncol* 2020, **38**(6)**:** 613-622.

26. Fennell DA, Danson S, Woll PJ, Forster M, Talbot D, Child J*, et al.* Ganetespib in Combination with Pemetrexed-Platinum Chemotherapy in Patients with Pleural Mesothelioma (MESO-02): A Phase Ib Trial. *Clin Cancer Res* 2020, **26**(18)**:** 4748-4755.

27. Ray-Coquard I, Braicu I, Berger R, Mahner S, Sehouli J, Pujade-Lauraine E*, et al.* Part I of GANNET53: A European Multicenter Phase I/II Trial of the Hsp90 Inhibitor Ganetespib Combined With Weekly Paclitaxel in Women With High-Grade, Platinum-Resistant Epithelial Ovarian Cancer-A Study of the GANNET53 Consortium. *Front Oncol* 2019, **9:** 832.

28. Obermayr E, Mohr T, Schuster E, Braicu EI, Taube E, Sehouli J*, et al.* Gene expression markers in peripheral blood and outcome in patients with platinum-resistant ovarian cancer: A study of the European GANNET53 consortium. *Int J Cancer* 2024, **155**(6)**:** 1128-1138.

29. Chou TC, Talalay P. Quantitative analysis of dose-effect relationships: the combined effects of multiple drugs or enzyme inhibitors. *Adv Enzyme Regul* 1984, **22:** 27-55.

30. Kabadi PK, Vantangoli MM, Rodd AL, Leary E, Madnick SJ, Morgan JR*, et al.* Into the depths: Techniques for in vitro three-dimensional microtissue visualization. *Biotechniques* 2015, **59**(5)**:** 279-286.

31. Kabadi PK, Rodd AL, Simmons AE, Messier NJ, Hurt RH, Kane AB. A novel human 3D lung microtissue model for nanoparticle-induced cell-matrix alterations. *Part Fibre Toxicol* 2019, **16**(1)**:** 15.

32. Galluzzi L, Vitale I, Michels J, Brenner C, Szabadkai G, Harel-Bellan A*, et al.* Systems biology of cisplatin resistance: past, present and future. *Cell Death Dis* 2014, **5**(5)**:** e1257.

33. Yue P, Han B, Zhao Y. Focus on the molecular mechanisms of cisplatin resistance based on multi-omics approaches. *Mol Omics* 2023, **19**(4)**:** 297-307.

34. Pokhriyal R, Hariprasad R, Kumar L, Hariprasad G. Chemotherapy Resistance in Advanced Ovarian Cancer Patients. *Biomark Cancer* 2019, **11:** 1179299X19860815.

35. Cutillas PR. Role of phosphoproteomics in the development of personalized cancer therapies. *Proteomics Clin Appl* 2015, **9**(3-4)**:** 383-395.

36. Qian L, Sun R, Xue Z, Guo T. Mass Spectrometry-Based Proteomics of Epithelial Ovarian Cancers: A Clinical Perspective. *Mol Cell Proteomics* 2023, **22**(7)**:** 100578.

37. Birbo B, Madu EE, Madu CO, Jain A, Lu Y. Role of HSP90 in Cancer. *Int J Mol Sci* 2021, **22**(19).

38. Concin N, Braicu I, Combe P, Berger R, Ray-Coquard I, Joly F*, et al.* GANNET53 Part II: A European Phase I/II Trial of the HSP90 inhibitor Ganetespib in high-grade Platinum-Resistant Ovarian Cancer - A Study of the GANNET53 consortium. *Clin Cancer Res* 2025, **31**(15):3160-3174.

39. N. Concin TVG, D. Lorusso, I.L. Ray-Coquard, A. Laenen, C. Zamagni, P. Harter, J. Sehouli, F. Raspagliesi, A.G. Zeimet, J-P. Lotz, V. Salutari, O. Tredan, R. Zeillinger, M. Dobbelstein, U. Moll, D. Kramer, E. Obermayr, I. Braicu, I.B. Vergote. European trial on enhanced DNA repair inhibition in ovarian cancer. *Annals of Oncology* 2024, **35:** 1.

40. Rastogi S, Joshi A, Sato N, Lee S, Lee MJ, Trepel JB*, et al.* An update on the status of HSP90 inhibitors in cancer clinical trials. *Cell Stress Chaperones* 2024, **29**(4)**:** 519-539.

41. Marques-Ramos A, Cervantes R. Expression of mTOR in normal and pathological conditions. *Mol Cancer* 2023, **22**(1)**:** 112.

42. Moschetta M, Reale A, Marasco C, Vacca A, Carratu MR. Therapeutic targeting of the mTOR-signalling pathway in cancer: benefits and limitations. *Br J Pharmacol* 2014, **171**(16)**:** 3801-3813.

43. Maharati A, Rajabloo Y, Moghbeli M. Molecular mechanisms of mTOR-mediated cisplatin response in tumor cells. *Heliyon* 2025, **11**(1)**:** e41483.

44. Zheng K, Gao Y, Xu J, Kang M, Chai R, Jin G*, et al.* mTOR Inhibitor Everolimus Modulates Tumor Growth in Small-Cell Carcinoma of the Ovary, Hypercalcemic Type and Augments the Drug Sensitivity of Cancer Cells to Cisplatin. *Biomedicines* 2024, **13**(1).

45. Zaja F, Federico M, Vitolo U, Zinzani PL. Management of relapsed/refractory mantle cell lymphoma: a review of current therapeutic strategies. *Leuk Lymphoma* 2014, **55**(5)**:** 988-998.

46. Kwitkowski VE, Prowell TM, Ibrahim A, Farrell AT, Justice R, Mitchell SS*, et al.* FDA approval summary: temsirolimus as treatment for advanced renal cell carcinoma. *Oncologist* 2010, **15**(4)**:** 428-435.

47. Farley JH, Brady WE, O'Malley D, Fujiwara K, Yonemori K, Bonebrake A*, et al.* A phase II evaluation of temsirolimus with carboplatin and paclitaxel followed by temsirolimus consolidation in clear cell ovarian cancer: An NRG oncology trial. *Gynecol Oncol* 2022, **167**(3)**:** 423-428.

48. Emons G, Kurzeder C, Schmalfeldt B, Neuser P, de Gregorio N, Pfisterer J*, et al.* Temsirolimus in women with platinum-refractory/resistant ovarian cancer or advanced/recurrent endometrial carcinoma. A phase II study of the AGO-study group (AGO-GYN8). *Gynecol Oncol* 2016, **140**(3)**:** 450-456.

49. Xie Y, Lei X, Zhao G, Guo R, Cui N. mTOR in programmed cell death and its therapeutic implications. *Cytokine Growth Factor Rev* 2023, **71-72:** 66-81.

50. Zou Z, Tao T, Li H, Zhu X. mTOR signaling pathway and mTOR inhibitors in cancer: progress and challenges. *Cell Biosci* 2020, **10:** 31.

51. Song M, Cui M, Liu K. Therapeutic strategies to overcome cisplatin resistance in ovarian cancer. *Eur J Med Chem* 2022, **232:** 114205.

52. Pan Z, Chen Y, Pang H, Wang X, Zhang Y, Xie X*, et al.* Design, synthesis, and biological evaluation of novel dual inhibitors of heat shock protein 90/mammalian target of rapamycin (Hsp90/mTOR) against bladder cancer cells. *Eur J Med Chem* 2022, **242:** 114674.

53. Piro G, Roca MS, Bruzzese F, Carbone C, Iannelli F, Leone A*, et al.* Vorinostat Potentiates 5-Fluorouracil/Cisplatin Combination by Inhibiting Chemotherapy-Induced EGFR Nuclear Translocation and Increasing Cisplatin Uptake. *Mol Cancer Ther* 2019, **18**(8)**:** 1405-1417.

54. Alfano L, Caporaso A, Altieri A, Dell'Aquila M, Landi C, Bini L*, et al.* Depletion of the RNA binding protein HNRNPD impairs homologous recombination by inhibiting DNA-end resection and inducing R-loop accumulation. *Nucleic Acids Res* 2019, **47**(8)**:** 4068-4085.

55. Gambelli A, Nespolo A, Rampioni Vinciguerra GL, Pivetta E, Pellarin I, Nicoloso MS*, et al.* Platinum-induced upregulation of ITGA6 promotes chemoresistance and spreading in ovarian cancer. *EMBO Mol Med* 2024, **16**(5)**:** 1162-1192.

56. Nespolo A, Stefenatti L, Pellarin I, Gambelli A, Rampioni Vinciguerra GL, Karimbayli J*, et al.* USP1 deubiquitinates PARP1 to regulate its trapping and PARylation activity. *Sci Adv* 2024, **10**(46)**:** eadp6567.

57. Iannelli F, Lombardi R, Costantini S, Roca MS, Addi L, Bruzzese F*, et al.* Integrated proteomics and metabolomics analyses reveal new insights into the antitumor effects of valproic acid plus simvastatin

combination in a prostate cancer xenograft model associated with downmodulation of YAP/TAZ signaling. *Cancer Cell Int* 2024, **24**(1)**:** 381.

58. Silva JC, Gorenstein MV, Li GZ, Vissers JP, Geromanos SJ. Absolute quantification of proteins by LCMSE: a virtue of parallel MS acquisition. *Mol Cell Proteomics* 2006, **5**(1)**:** 144-156.

59. Tyanova S, Temu T, Sinitcyn P, Carlson A, Hein MY, Geiger T*, et al.* The Perseus computational platform for comprehensive analysis of (prote)omics data. *Nat Methods* 2016, **13**(9)**:** 731-740.

60. Huang da W, Sherman BT, Lempicki RA. Systematic and integrative analysis of large gene lists using DAVID bioinformatics resources. *Nat Protoc* 2009, **4**(1)**:** 44-57.

61. Raudvere U, Kolberg L, Kuzmin I, Arak T, Adler P, Peterson H*, et al.* g:Profiler: a web server for functional enrichment analysis and conversions of gene lists (2019 update). *Nucleic Acids Res* 2019, **47**(W1)**:** W191-W198.

62. Bruzzese F, Rocco M, Castelli S, Di Gennaro E, Desideri A, Budillon A. Synergistic antitumor effect between vorinostat and topotecan in small cell lung cancer cells is mediated by generation of reactive oxygen species and DNA damage-induced apoptosis. *Mol Cancer Ther* 2009, **8**(11)**:** 3075-3087.

63. Terranova-Barberio M, Roca MS, Zotti AI, Leone A, Bruzzese F, Vitagliano C*, et al.* Valproic acid potentiates the anticancer activity of capecitabine in vitro and in vivo in breast cancer models via induction of thymidine phosphorylase expression. *Oncotarget* 2016, **7**(7)**:** 7715-7731.

Figure legends

Fig. 1. Label-free LC-MS/MS-based phosphoproteomics quantification and bioinformatics analysis. A Unsupervised multivariate analysis (PCA plot) showed good experimental reproducibility as demonstrated by the close relation between the three biological replicates of parental (TOV-112D) and resistant cells (TOV-112D Pt-rescl.7). The six spot maps for each cell line clearly clustered into two groups corresponding to Pt-res cells (red) *vs* parental cells (black; $P < 0.05$). P-values were calculated based on unpaired Student's t-test. **B** Gene set enrichment analysis using g:Profiler (https://biit.cs.ut.ee/gprofiler/). The significantly changed terms enriched by GO, Reactome (REAC), Wikipathways (WP) and Human Protein Atlas (HPA). **C, D** Functional enrichment analysis of the significant proteins using DAVID software in terms of KEGG pathways and functional annotation clustering.

Fig 2. Schematic representation of the main investigated pathways and western blot validation experiments of the identified phosphoproteins. A Upon receptor binding by growth factors and cytokines, phosphatidylinositol 3-kinase (PI3K) is activated and in turn phosphorylates PDK1 and AKT, witch activate mTOR by phosphorylation. mTOR phosphorylates downstream p70S6K which activatesRPS6 promoting tumor proliferation. Moreover, mTOR or DYRK2 directly activates HSF1 protein by phosphorylation, promoting its nuclear translocation and transcription of HSP genes. **B** Western blot analysis, performed after 48h of cell culture, showed an activation of mTOR mediated signalling pathway thorough the phosphorilation of p^{S241}-PDK1, p^{S473}-AKT, p^{S2448}-mTOR, p^{THR389}-p70S6K, $p^{S235/236}$RPS6 proteins in TOV-112D Pt-res cl.7 resistant cells *vs*TOV-112D parental cells (Par). Densitometric analysis was done by ImageJ software and reported as the ratio: phospho-protein/total protein/loading control (ß-actin). **C** HSF1 dependent transactivation was confirmed by western blot

analysis performed after 48h of cell culture, showing an upregulation of $p^{TYR386/268}$-DYRK2 and p^{S326}-HSF1 proteins in TOV-112D Pt-res cl.7 resistant cells compared with TOV-112D parental cells (Par). Densitometric analysis was done by ImageJ software and reported as ratio: phospho-protein/total protein/loading control (ß-actin). **D** Expression of the proteins of chaperone complex (HSP90α, HSP90β, HSP40, HSP70) was evaluated by western blot experiment in TOV-112D Pt-res cl.7 resistant cells *vs* TOV-112D parental cells (Par) performed after 48h of cell culture. Densitometric analysis was done by ImageJ software and reported as ratio relative to the indicated loading control (ß-actin). **E** Expression of p^{S2448}-mTOR, p^{S326}-HSF1 and HSP90α was evaluated by western blot experiment in Pt-resistant primary cells compared to Pt-sensitive primary cells performed after 48h of cell culture. Densitometric analysis values are reported as ratios relative to the corresponding β-actin levels.

Fig 3. Effect of HSP90α knock-in in platinum-sensitive TOV-112D cells. A Western blot analysis evaluating the expression of Flag-HSP90α in TOV-112D empty vector and TOV-112D over expressing HSP90α (Flag-HSP90α). β-Actin was used as loading control. Western blot quantification was performed by ImageJsoftware. **B** Clonogenic assay of TOV112-D empty vector and TOV-112D Flag-HSP90α cells treated with CDDP at the IC_{10}^{96h} for parental cells. Representative data of at least three independent experiments performed in triplicates. Statistically significant results are reported (****P < 0.0001, ns, not statistically significant). **C** Apoptosis and necrosis evaluated by flow cytometry after Annexin V-FITC and propidium iodide staining in TOV-112D empty vector and and TOV-112D Flag- HSP90α, untreated or treated with CDDP for 48h with CDDP at IC_{50}^{96h} doses of parental cells. **D** Western blot analysis of γH2AX expression in TOV-112D empty vector and and TOV-112D Flag-HSP90α, untreated or treated with CDDP for 48h at IC_{50}^{96h} doses of parental cells.

Fig 4. Potentiation of CDDP antitumor effect induced by ganetespib and temsirolimus in parental and Pt-resistant TOV-112D cells. A CI (combination index) values (mean ± SD from at least three separate experiments performed in quadruplicates) computed at 50% (CI50), 75% (CI75) and 90% (CI90) of cell kill by CalcuSyn software after 96h for TOV-112D and TOV-112D Pt-res cl.7 cells. The treatments are indicated in the figure. The combinations were considered synergistic when CIs were below 0.9, additive when CIs were between 0.9 and 1.1 or antagonism when Cis were more than 1.1. **B** DRI (doses reduction index) values (mean ± SD) for CDDP from at least three separate experiments performed in quadruplicate) that represent the order of magnitude (fold) of dose reduction obtained for IC50 (DRI50) in combination setting compared with each drug alone in TOV-112D and TOV-112D Pt-res cl.7 cells. **C** Synergistic inhibition of colony formationin TOV-112D and TOV-112D Pt-res cl.7 treated with CDDP, ganetespib, temsirolimus or their combination (simultaneous exposure) at the IC_{10}^{96h} doses for parental cells. Representative data of at least three independent experiments performed in triplicates. Statistically significant results calculated with one-way ANOVA test are reported (a indicates control group, b indicates CDDP-treated cells, and c indicates ganetespib-treated cells, d indicates temsirolimus-treated cells, e indicates cddp plus ganetespib-treated cells *P < 0.05, **P < 0.01, ***P < 0.001 and ****P < 0.0001, ns, not statistically significant). **D** Synergistic inhibition of microtissues formation by CDDP, ganetespib, temsirolimus alone and in combination. Cancer cells (red ones-marked by cell tracker) and mice fibroblast cellsNIH/3T3 were plated in each well and after 24h treated withIC_{50}^{96h} doses of parental cells. Representative images from Opera Phenix confocal microscopy. The graphics represent the number of viable cells in 3D cell culture based on quantitation of the ATP content. Results were obtained by a single experiment performed in triplicate (±SD). Statistically significant results calculated with one-way ANOVA test are reported (a indicates control group, b indicates CDDP-treated cells, and c indicates ganetespib-treated cells, d indicates temsirolimus-treated cells, e indicates CDDP plus ganetespib-treated cells *P < 0.05, **P < 0.01, ***P < 0.001 and ****P < 0.0001, ns, not statistically significant).

Fig 5. Pro-apoptotic and DNA damage effect of ganetespib and temsirolimus plus CDDP in EOC cells. A Apoptosis and necrosis evaluated by flow cytometry after Annexin V-FITC and propidium iodide staining in TOV-112D and TOV-112D Pt-res cl. 7, untreated or treated for 24h or 48h, with temsirolimus,

CDDP plus ganetespib and CDDP plus ganetespib and temsirolimus at IC_{50}^{96h} doses of parental cells. **B** Western blot analysis of cleaved PARP1in TOV-112D and TOV-112D Pt-res cl. 7 cells untreated or treated with CDDP, ganetespib, temsirolimus and their combinationat IC_{50}^{96h} doses of parental cells at the time indicated above. β-actin expression serves as loading control. Western blot quantification was performed by ImageJ software. **C** Western blot analysis of γH2AX in TOV-112D and TOV-112D Pt-res cl. 7 cells untreated or treated with CDDP, ganetespib, temsirolimus and their combination at IC_{50}^{96h} doses of parental cells at the time indicated above. β-actin expression serves as loading control. Western blot quantification was performed by ImageJ software.

Fig 6. Effect of the triple combination on the main investigated pathways in Pt-res EOC cells.
A-C Western blot analysis, performed after 48h of treatment, of the main proteins (indicated in the figure) involved in mTOR mediated signalling pathway (**A**), HSF1 dependent transactivation (**B**) and chaperone complex (**C**) in TOV-112D Pt-res cl. 7 cells untreated or treated with CDDP, ganetespib, temsirolimus and their combination at IC_{50}^{96h} doses of parental cells. β-actin expression serves as loading control. Western blot quantification was performed by ImageJ software.

Fig 7. Potentiation of CDDP antitumor effect induced by ganetespib and temsirolimus *in vivo* Pt-resistant TOV-112D xenograft model. A Schematic of the *in vivo* xenograft experiment, including timeline and agent concentration. TOV-112D Pt-res cl.7 cells (6×10^6) were s.c. injected into NSG mice as described in Materials and Methods. When tumors were established, mice were treated once a week for two weeks with vehicles (CTR) or temsirolimus (20 mg·kg−1 i.p.) or CDDP (2.5 mg·kg−1 i.p.) and ganetespib (GANE; 30 mg·kg−1 i.p.) or triple CDDP/ganetespib/temsirolimus combination. **B** Relative tumor volume (TV) measured at prespecified time points (Means ± SEM). **C** Mice body weight as surrogate indicator of toxicity for *in vivo* experiment reported in A. Body weight was measured three times/week. **D** TGD, indicating the mean rate of tumor growth in the treatment groups relative to control untreated mice (see Materials and Methods). **E** Percent change in tumor volume average from first day of treatment (day 0) to day 28 for each treatment group compared to vehicles group. **F** Kaplan–Meier curves comparing the survival of single and combination groups of treatment. Statistically significant results calculated with one-way ANOVA test comparing ganetespib plus CDDP and ganetespib/temsirolimus plus CDDP are reported (*$P < 0.05$ and ****$P < 0.0001$).

A

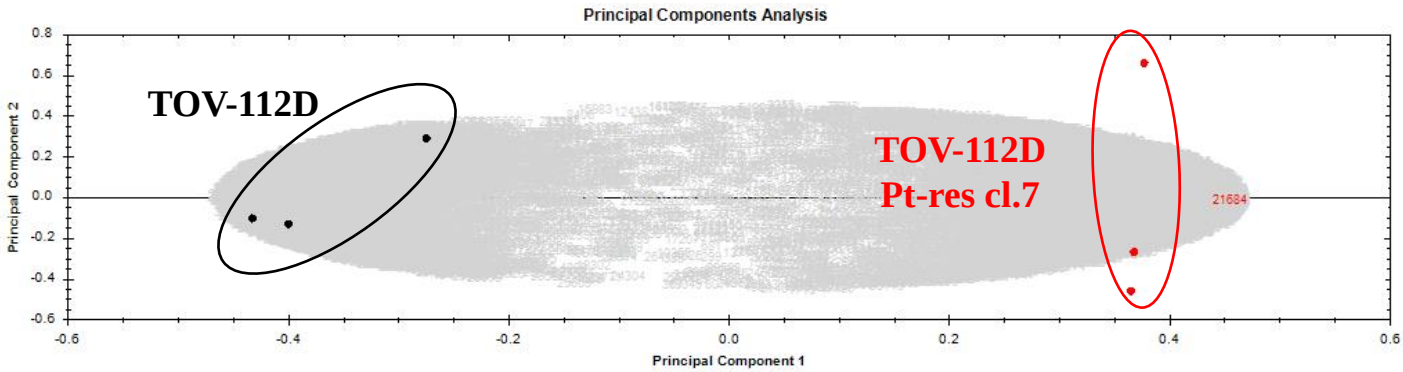
Principal Components Analysis
TOV-112D
TOV-112D
Pt-res cl.7
Principal Component 2
Principal Component 1
21684

B

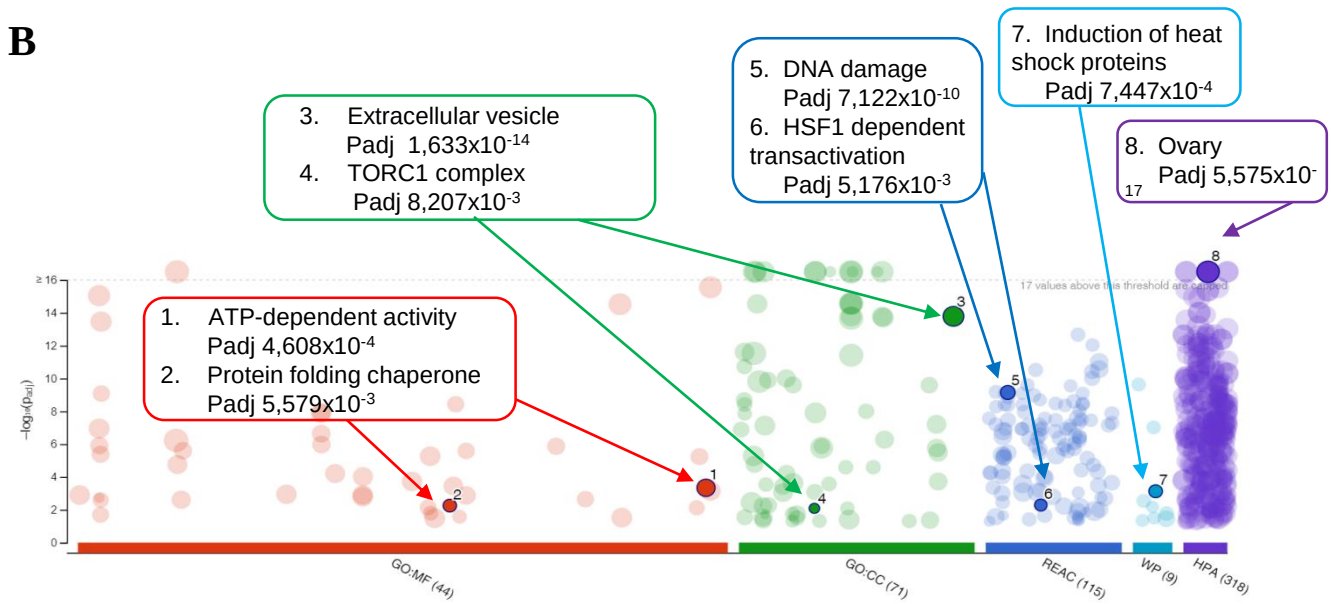
1. ATP-dependent activity
Padj 4,608x10-4
2. Protein folding chaperone
Padj 5,579x10-3
3. Extracellular vesicle
Padj 1,633x10-14
4. TORC1 complex
Padj 8,207x10-3
5. DNA damage
Padj 7,122x10-10
6. HSF1 dependent transactivation
Padj 5,176x10-3
7. Induction of heat shock proteins
Padj 7,447x10-4
8. Ovary
Padj 5,575x10-17
GO:MF (44)
GO:CC (71)
REAC (115)
WP (9)
HPA (318)

C

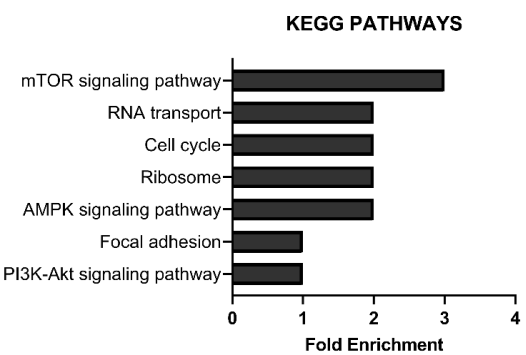
KEGG PATHWAYS
mTOR signaling pathway
RNA transport
Cell cycle
Ribosome
AMPK signaling pathway
Focal adhesion
PI3K-Akt signaling pathway
Fold Enrichment

D

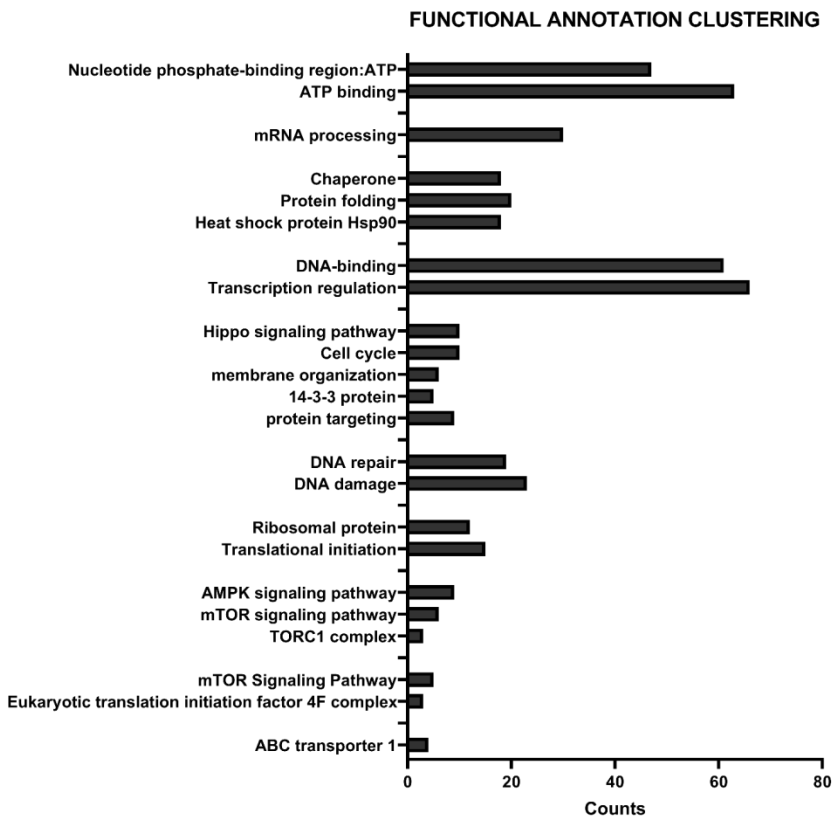
FUNCTIONAL ANNOTATION CLUSTERING
Nucleotide phosphate-binding region:ATP
ATP binding
mRNA processing
Chaperone
Protein folding
Heat shock protein Hsp90
DNA-binding
Transcription regulation
Hippo signaling pathway
Cell cycle
membrane organization
14-3-3 protein
protein targeting
DNA repair
DNA damage
Ribosomal protein
Translational initiation
AMPK signaling pathway
mTOR signaling pathway
TORC1 complex
mTOR Signaling Pathway
Eukaryotic translation initiation factor 4F complex
ABC transporter 1
Counts

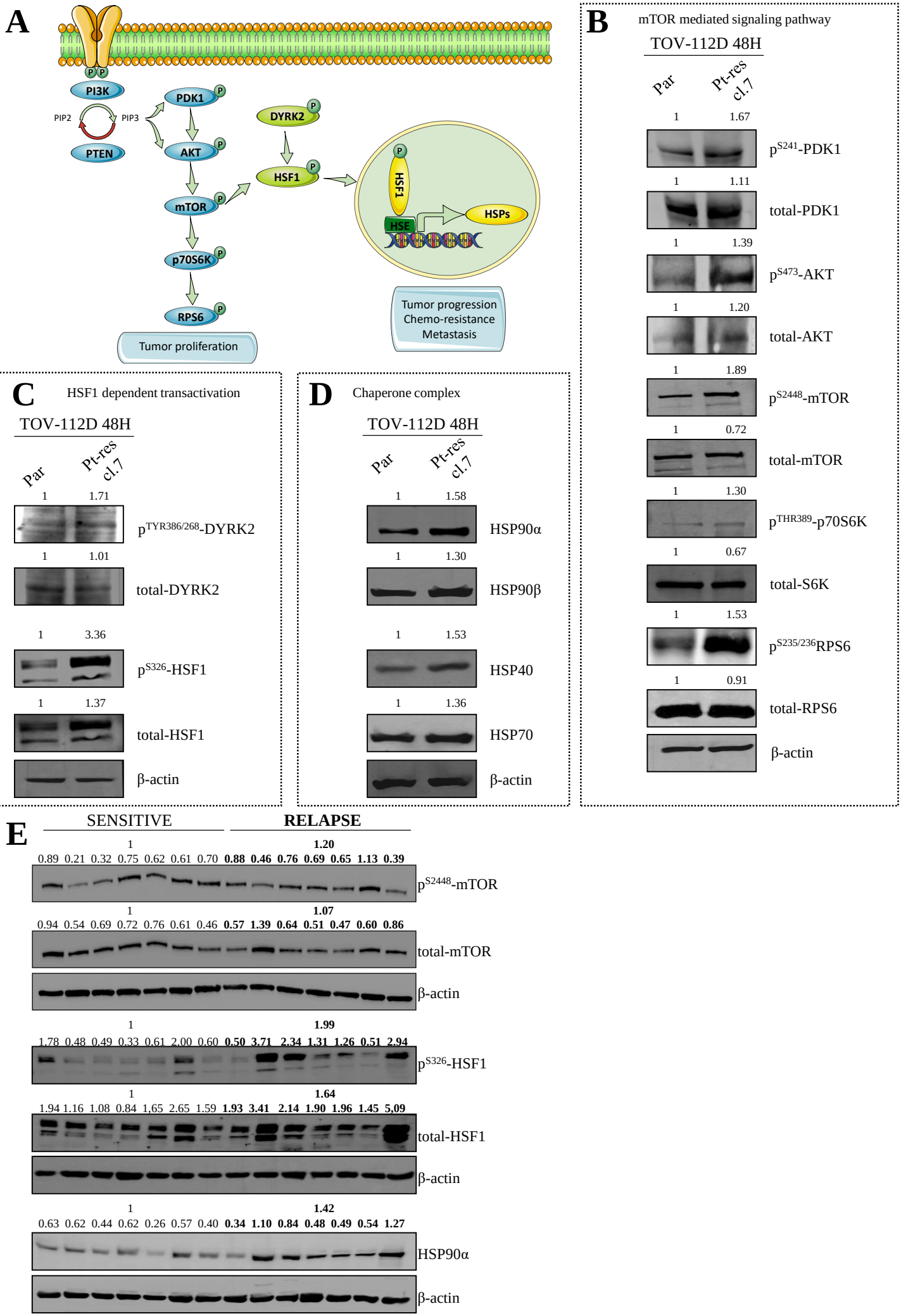
A
PI3K
PIP2
PIP3
PTEN
PDK1
AKT
mTOR
p70S6K
RPS6
Tumor proliferation
DYRK2
HSF1
HSF1
HSE
HSPs
Tumor progression
Chemo-resistance
Metastasis
B
mTOR mediated signaling pathway
TOV-112D 48H
Par
Pt-res cl.7
1 1.67
pS241-PDK1
1 1.11
total-PDK1
1 1.39
pS473-AKT
1 1.20
total-AKT
1 1.89
pS2448-mTOR
1 0.72
total-mTOR
1 1.30
pTHR389-p70S6K
1 0.67
total-S6K
1 1.53
pS235/236RPS6
1 0.91
total-RPS6
β-actin
C
HSF1 dependent transactivation
TOV-112D 48H
Par
Pt-res cl.7
1 1.71
pTYR386/268-DYRK2
1 1.01
total-DYRK2
1 3.36
pS326-HSF1
1 1.37
total-HSF1
β-actin
D
Chaperone complex
TOV-112D 48H
Par
Pt-res cl.7
1 1.58
HSP90α
1 1.30
HSP90β
1 1.53
HSP40
1 1.36
HSP70
β-actin
E
SENSITIVE
RELAPSE
1 1.20
0.89 0.21 0.32 0.75 0.62 0.61 0.70 0.88 0.46 0.76 0.69 0.65 1.13 0.39
pS2448-mTOR
1 1.07
0.94 0.54 0.69 0.72 0.76 0.61 0.46 0.57 1.39 0.64 0.51 0.47 0.60 0.86
total-mTOR
β-actin
1 1.99
1.78 0.48 0.49 0.33 0.61 2.00 0.60 0.50 3.71 2.34 1.31 1.26 0.51 2.94
pS326-HSF1
1 1.64
1.94 1.16 1.08 0.84 1,65 2.65 1.59 1.93 3.41 2.14 1.90 1.96 1.45 5,09
total-HSF1
β-actin
1 1.42
0.63 0.62 0.44 0.62 0.26 0.57 0.40 0.34 1.10 0.84 0.48 0.49 0.54 1.27
HSP90α
β-actin

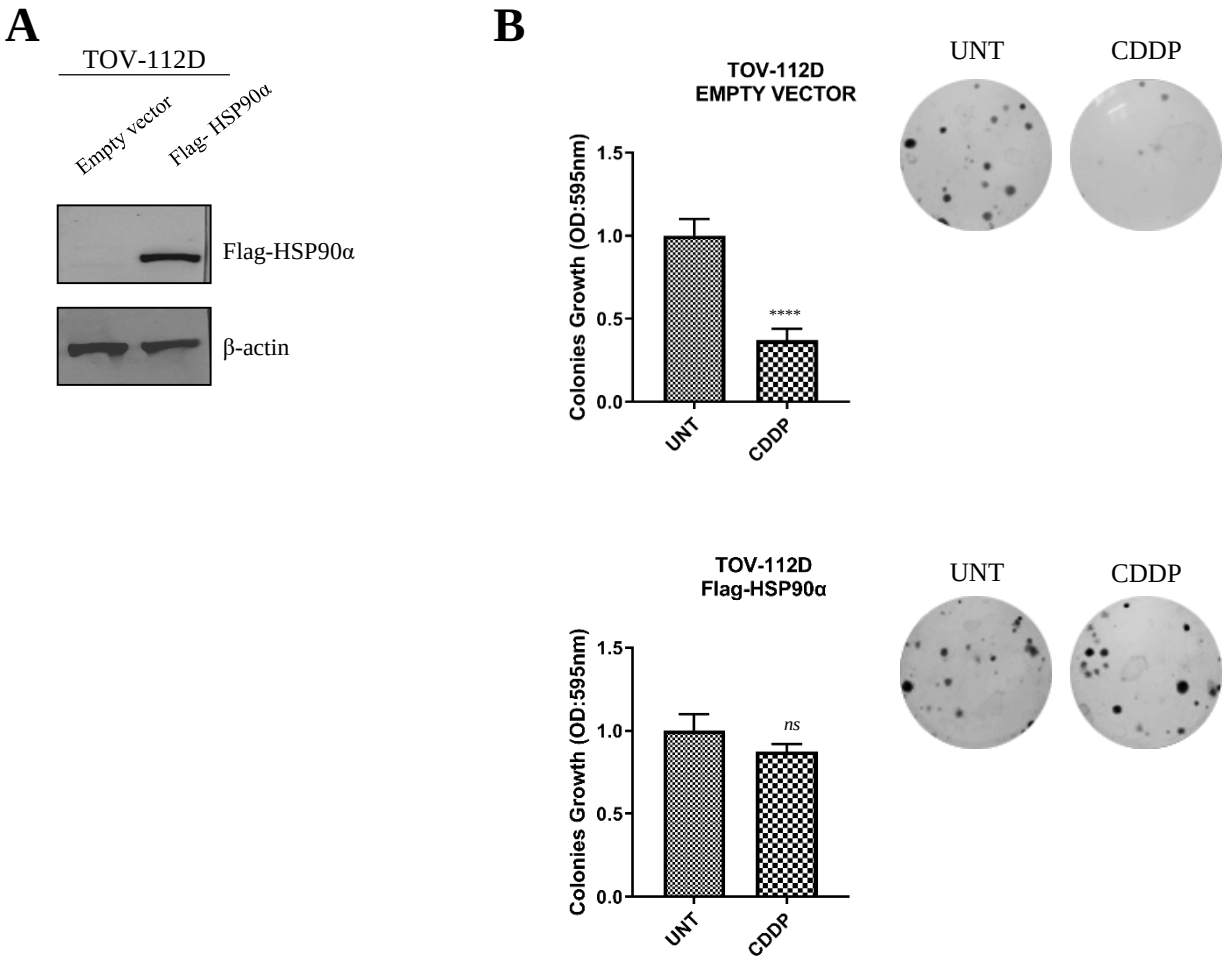
A
TOV-112D
Empty vector
Flag- HSP90α
Flag-HSP90α
β-actin
B
TOV-112D
EMPTY VECTOR
UNT
CDDP
Colonies Growth (OD:595nm)
1.5
1.0
0.5
0.0
****
UNT
CDDP
TOV-112D
Flag-HSP90α
UNT
CDDP
Colonies Growth (OD:595nm)
1.5
1.0
0.5
0.0
ns
UNT
CDDP

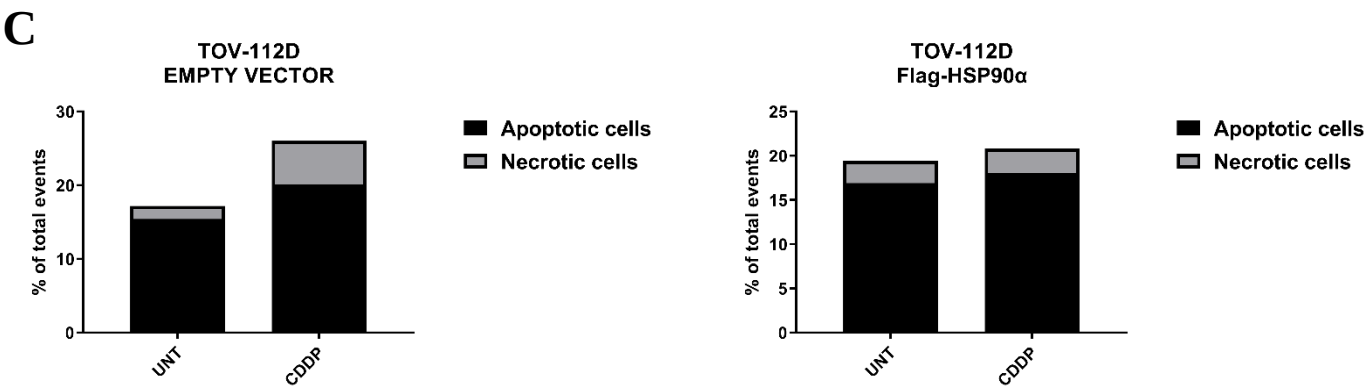
C
TOV-112D
EMPTY VECTOR
% of total events
30
20
10
0
Apoptotic cells
Necrotic cells
UNT
CDDP
TOV-112D
Flag-HSP90α
% of total events
25
20
15
10
5
0
Apoptotic cells
Necrotic cells
UNT
CDDP


D
TOV-112D
EMPTY VECTOR
UNT
CDDP
1
1.99
γH2AX
β-actin
TOV-112D
Flag-HSP90α
UNT
CDDP
1
1.10
γH2AX
β-actin

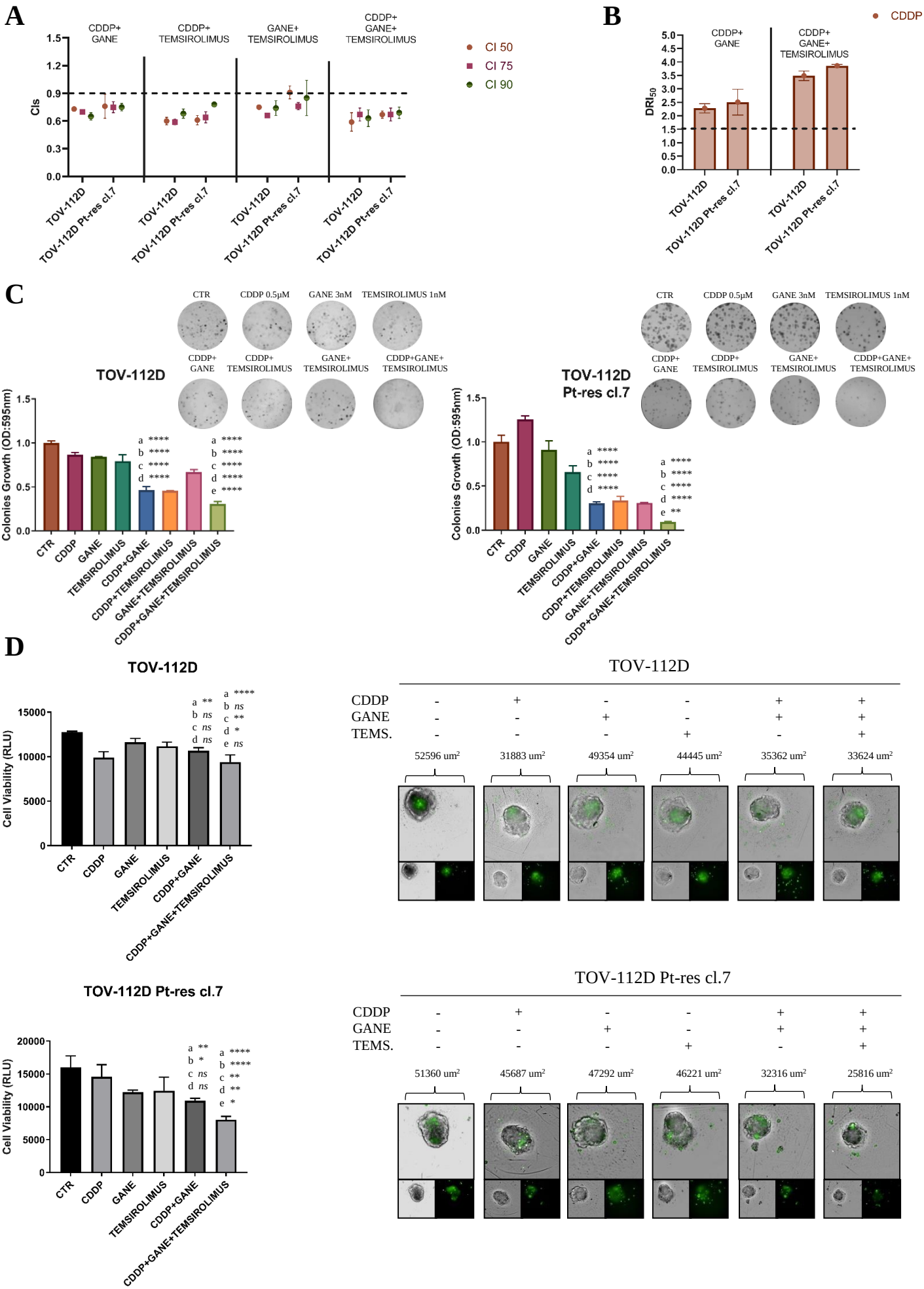
A
CDDP+ GANE
CDDP+ TEMSIROLIMUS
GANE+ TEMSIROLIMUS
CDDP+ GANE+ TEMSIROLIMUS
CIs
CI 50
CI 75
CI 90
TOV-112D
TOV-112D Pt-res cl.7
B
CDDP
DRI50
C
CTR
CDDP 0.5µM
GANE 3nM
TEMSIROLIMUS 1nM
TOV-112D
TOV-112D Pt-res cl.7
Colonies Growth (OD:595nm)
CTR
CDDP
GANE
TEMSIROLIMUS
CDDP+GANE
CDDP+TEMSIROLIMUS
GANE+TEMSIROLIMUS
CDDP+GANE+TEMSIROLIMUS
D
TOV-112D
Cell Viability (RLU)
TOV-112D Pt-res cl.7
CDDP
GANE
TEMS.
52596 um²
31883 um²
49354 um²
44445 um²
35362 um²
33624 um²
51360 um²
45687 um²
47292 um²
46221 um²
32316 um²
25816 um²

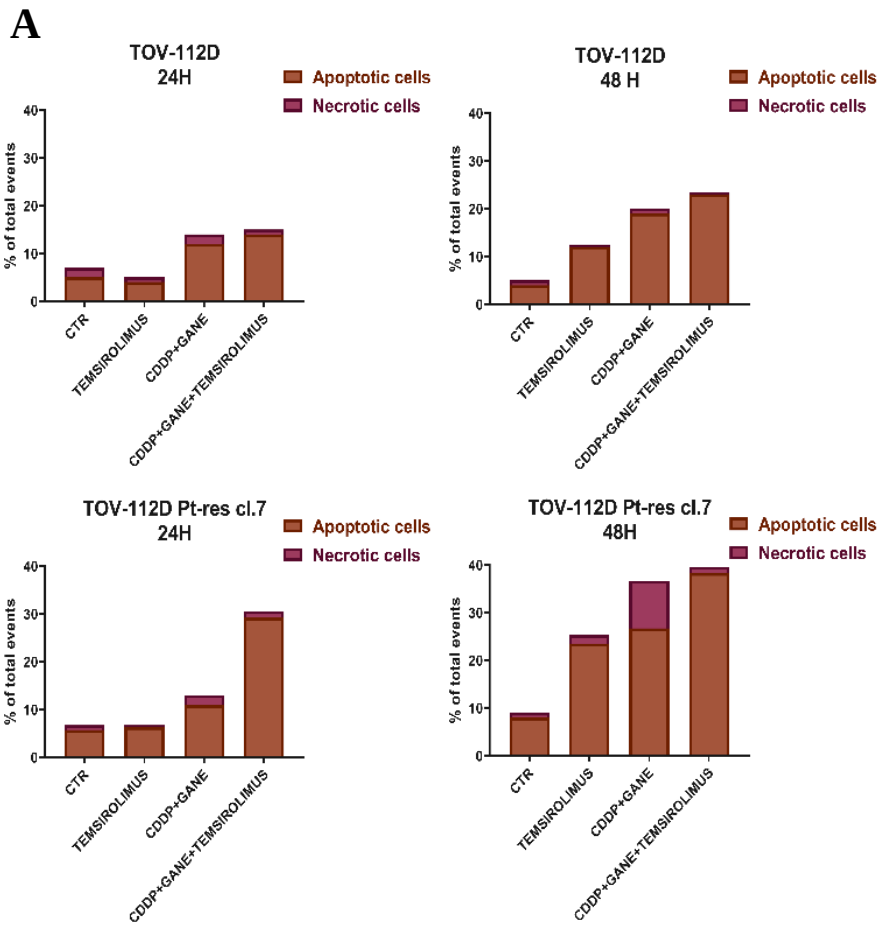
A
TOV-112D
24H
Apoptotic cells
Necrotic cells
% of total events
CTR
TEMSIROLIMUS
CDDP+GANE
CDDP+GANE+TEMSIROLIMUS
TOV-112D
48 H
TOV-112D Pt-res cl.7
24H
TOV-112D Pt-res cl.7
48H

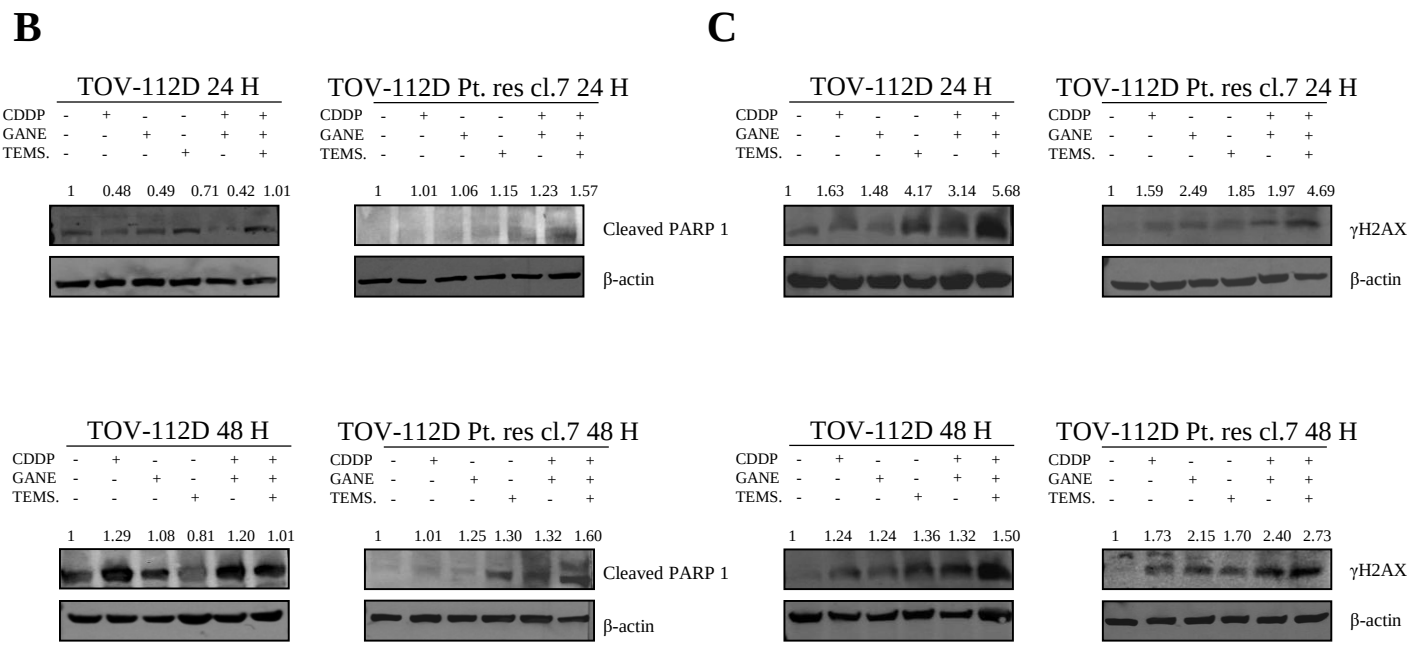
B
TOV-112D 24 H
TOV-112D Pt. res cl.7 24 H
CDDP
GANE
TEMS.
1 0.48 0.49 0.71 0.42 1.01
1 1.01 1.06 1.15 1.23 1.57
Cleaved PARP 1
β-actin
C
TOV-112D 24 H
TOV-112D Pt. res cl.7 24 H
1 1.63 1.48 4.17 3.14 5.68
1 1.59 2.49 1.85 1.97 4.69
γH2AX
β-actin

TOV-112D 48 H
TOV-112D Pt. res cl.7 48 H
CDDP
GANE
TEMS.
1 1.29 1.08 0.81 1.20 1.01
1 1.01 1.25 1.30 1.32 1.60
Cleaved PARP 1
β-actin
TOV-112D 48 H
TOV-112D Pt. res cl.7 48 H
1 1.24 1.24 1.36 1.32 1.50
1 1.73 2.15 1.70 2.40 2.73
γH2AX
β-actin

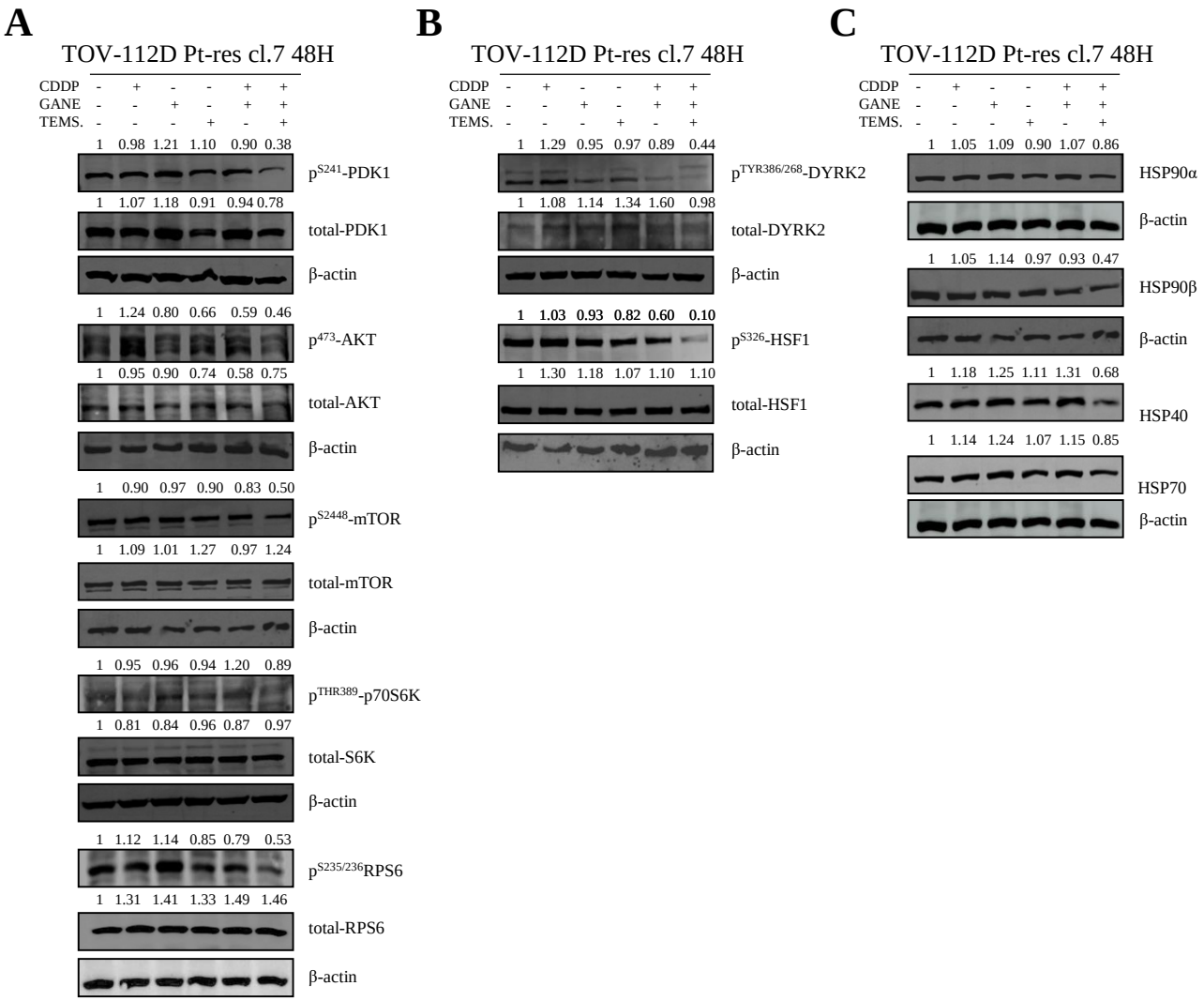
A
TOV-112D Pt-res cl.7 48H
CDDP - + - - + +
GANE - - + - + +
TEMS. - - - + - +
1 0.98 1.21 1.10 0.90 0.38
pS241-PDK1
1 1.07 1.18 0.91 0.94 0.78
total-PDK1
β-actin
1 1.24 0.80 0.66 0.59 0.46
p473-AKT
1 0.95 0.90 0.74 0.58 0.75
total-AKT
β-actin
1 0.90 0.97 0.90 0.83 0.50
pS2448-mTOR
1 1.09 1.01 1.27 0.97 1.24
total-mTOR
β-actin
1 0.95 0.96 0.94 1.20 0.89
pTHR389-p70S6K
1 0.81 0.84 0.96 0.87 0.97
total-S6K
β-actin
1 1.12 1.14 0.85 0.79 0.53
pS235/236RPS6
1 1.31 1.41 1.33 1.49 1.46
total-RPS6
β-actin
B
TOV-112D Pt-res cl.7 48H
CDDP - + - - + +
GANE - - + - + +
TEMS. - - - + - +
1 1.29 0.95 0.97 0.89 0.44
pTYR386/268-DYRK2
1 1.08 1.14 1.34 1.60 0.98
total-DYRK2
β-actin
1 1.03 0.93 0.82 0.60 0.10
pS326-HSF1
1 1.30 1.18 1.07 1.10 1.10
total-HSF1
β-actin
C
TOV-112D Pt-res cl.7 48H
CDDP - + - - + +
GANE - - + - + +
TEMS. - - - + - +
1 1.05 1.09 0.90 1.07 0.86
HSP90α
β-actin
1 1.05 1.14 0.97 0.93 0.47
HSP90β
β-actin
1 1.18 1.25 1.11 1.31 0.68
HSP40
1 1.14 1.24 1.07 1.15 0.85
HSP70
β-actin

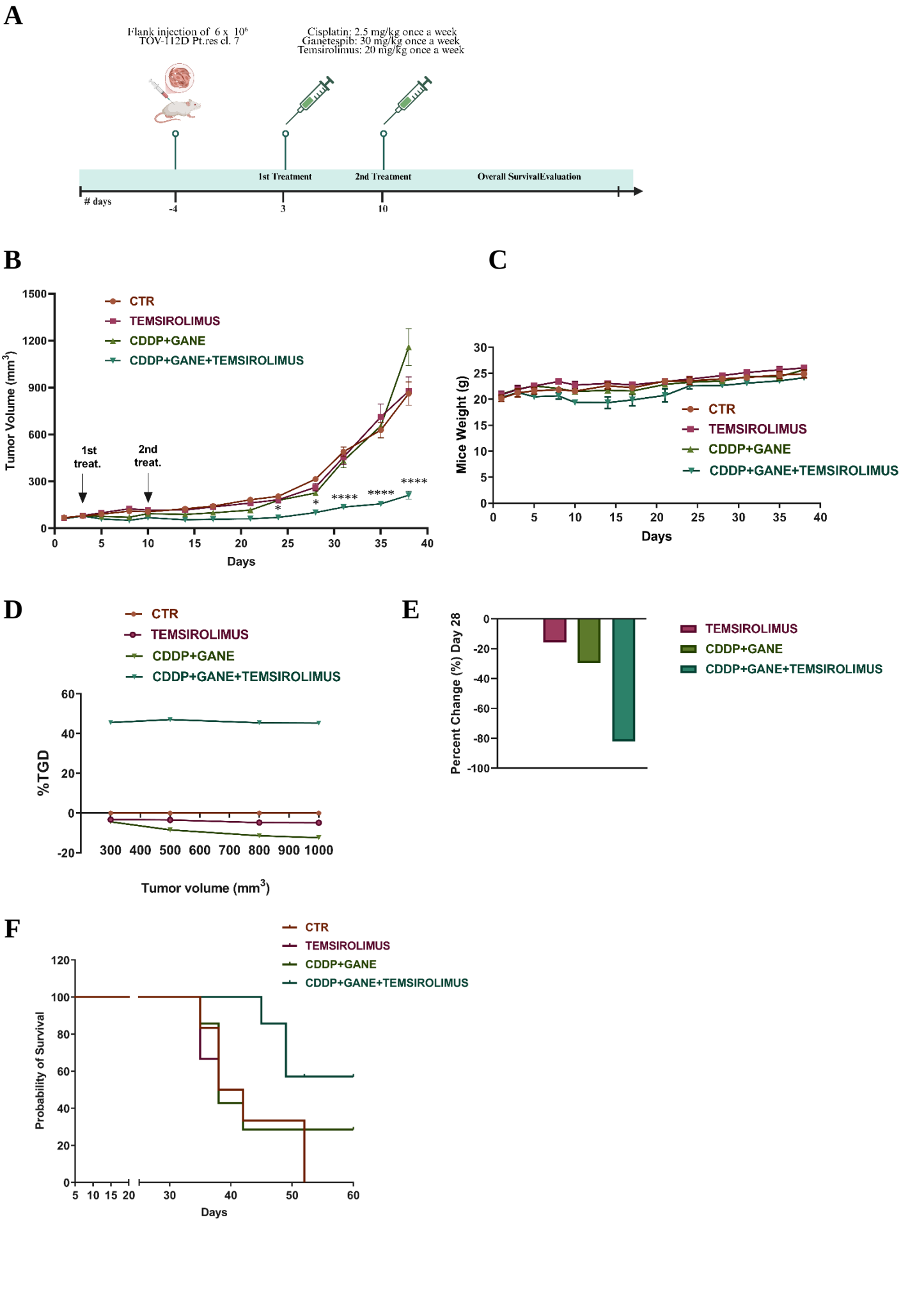
A
Flank injection of 6 x 10⁶
TOV-112D Pt.res cl. 7
Cisplatin: 2.5 mg/kg once a week
Ganetespib: 30 mg/kg once a week
Temsirolimus: 20 mg/kg once a week
1st Treatment
2nd Treatment
Overall SurvivalEvaluation
days
-4
3
10
B
CTR
TEMSIROLIMUS
CDDP+GANE
CDDP+GANE+TEMSIROLIMUS
Tumor Volume (mm3)
1st treat.
2nd treat.
Days
C
Mice Weight (g)
Days
D
%TGD
Tumor volume (mm3)
E
Percent Change (%) Day 28
F
Probability of Survival
Days